APPLICATION OF A NATURAL-RESONANCE BASED FEATURE EXTRACTION TECHNIQUE TO SMALL-SCALE AIRCRAFT MODELED BY CONDUCTING WIRES FOR ELECTROMAGNETIC TARGET CLASSIFICATION

A THESIS SUBMITTED TO
THE GRADUATE SCHOOL OF NATURAL AND APPLIED SCIENCES
OF
MIDDLE EAST TECHNICAL UNIVERSITY

BY

MEHMET OKAN ERSOY

IN PARTIAL FULFILLMENT OF THE REQUIREMENTS
FOR
THE DEGREE OF MASTER OF SCIENCE
IN
ELECTRICAL AND ELECTRONICS ENGINEERING

SEPTEMBER 2004

Approval of the Graduate School of Natural And Applied Sciences

Prof. Dr. Canan Özgen
Director

I certify that this thesis satisfies all the requirements as a thesis for the degree of Master of Science.

Prof. Dr. Mübeccel Demirekler
Head of Department

This is to certify that we have read this thesis and that in our opinion it is fully adequate, in scope and quality, as a thesis for the degree of Master of Science.

Prof. Dr. Gönül Turhan Sayan
Supervisor

Examining Committee Members

Prof. Dr. Mustafa Kuzuoğlu (ODTÜ, EE)

Prof. Dr. Gönül Turhan Sayan (ODTÜ, EE)

Prof. Dr. Kemal Leblebicioğlu (ODTÜ, EE)

Assoc. Prof. Dr. Gülbin Dural (ODTÜ, EE)

Asst. Prof. Dr. Erkan Afacan (Gazi Unv., EE)

I hereby declare that all information in this document has been obtained and presented in accordance with academic rules and ethical conduct. I also declare that, as required by these rules and conduct, I have fully cited and referenced all material and results that are not original to this work.

Name, Last name: Mehmet Okan, Ersoy

Signature :

ABSTRACT

APPLICATION OF A NATURAL-RESONANCE BASED FEATURE EXTRACTION TECHNIQUE TO SMALL-SCALE AIRCRAFT MODELED BY CONDUCTING WIRES FOR ELECTROMAGNETIC TARGET CLASSIFICATION

Ersoy, Mehmet Okan
M.Sc., Department of Electrical and Electronics Engineering
Supervisor: Prof. Dr. Gönül Turhan Sayan

September 2004, 89 pages

The problem studied in this thesis, is the classification of the small-scale aircraft targets by using a natural resonance based electromagnetic feature extraction technique. The aircraft targets are modeled by perfectly conducting, thin wire structures. The electromagnetic back-scattered data used in the classification process, are numerically generated for five aircraft models.

A contemporary signal processing tool, the Wigner-Ville distribution is employed in this study in addition to using the principal components analysis technique to extract target features mainly from late-time target responses. The Wigner-Ville distribution (WD) is applied to the electromagnetic back-scattered responses from different aspects. Then, feature vectors are extracted from suitably chosen late-time portions of the WD outputs, which include natural resonance related

information, for every target and aspect to decrease aspect dependency. The database of the classifier is constructed by the feature vectors extracted at only a few reference aspects. Principal components analysis is also used to fuse the feature vectors and/or late-time aircraft responses extracted from reference aspects of a given target into a single characteristic feature vector of that target to further reduce aspect dependency. Consequently, an almost aspect independent classifier is designed for small-scale aircraft targets reaching high correct classification rate.

Keywords: Natural resonance, feature extraction, electromagnetic target classification, time-frequency analysis, Wigner-Ville distribution, principal component analysis

ÖZ

ELEKTROMANYETİK HEDEF SINIFLANDIRMA AMACIYLA, DOĞAL RESONANSLARA DAYALI BİR ÖZNİTELİK ÇIKARIM TEKNİĞİNİN İLETKEN TELLERLE MODELLENMİŞ KÜÇÜK ÖLÇEKLİ UÇAKLARA UYGULANMASI

Ersoy, Mehmet Okan
Yüksek Lisans, Elektrik-Elektronik Mühendisliği Bölümü
Tez Yöneticisi: Prof. Dr. Gönül Turhan Sayan

Eylül 2004, 89 sayfa

Bu tezde, doğal rezonanslara dayalı bir elektromanyetik hedef öznitelik çıkarım tekniği kullanılarak, küçük ölçekli uçak hedeflerinin sınıflandırılması problemi incelenmiştir. Uçak hedefleri ince, mükemmel iletken tel yapılarla modellenmiştir. Sınıflandırma işleminde kullanılan, beş uçak modelinden geri saçılan elektromanyetik alanlar, nümerik olarak üretilmiştir.

Bu çalışmada, hedeflerin geç zaman tepkilerinden özniteliklerini çıkarmak amacıyla, esas bileşenler analizi tekniğinin yanı sıra bir güncel sinyal işleme aracı olan Wigner-Ville dağılımı kullanılmıştır. Farklı açılardan geri saçılan elektromanyetik tepkilere Wigner-Ville dağılımı (WD) uygulanmıştır. Açısal bağımlılığı azaltmak amacıyla, her hedef ve açı için, WD sonuçlarının uygun olarak seçilmiş, doğal rezonanslarla ilgili bilgileri içeren geç zaman bölgelerinden bir öz

nitelik vektörü çıkarılmıştır. Hedef sınıflandırıcının veri tabanı, çok az sayıda referans açısındaki hedef tepkilerinden çıkartılan öznitelik vektörlerinden oluşturulmuştur. Esas bileşenler tekniği, açısal bağımlılığı daha da düşürmek amacıyla, bir hedef için referans açılarında üretilmiş öz nitelik vektörlerinin ve/veya geç zaman uçak tepkilerinin, hedefi tanımlayan tek bir öz nitelik vektöründe toplanmasında kullanılmıştır. Böylece, görüş açısından mümkün olduğunca bağımsız bir hedef sınıflandırıcı küçük ölçekli uçak hedefleri için dizayn edilmiş ve yüksek doğru sınıflandırma oranına ulaşılmıştır.

Anahtar Kelimeler: Doğal rezonans, öznitelik çıkarımı, elektromanyetik hedef sınıflandırma, zaman-frekans analizi, Wigner-Ville dağılımı, esas bileşenler analizi

Devoted to the unforgettable memory of my father, Aydın Ersoy

ACKNOWLEDGMENTS

The author wishes to express his deepest gratitude to his supervisor, Prof. Dr. Gönül Turhan Sayan for her guidance, advice, criticism, encouragement and insight throughout the research.

TABLE OF CONTENTS

LIST OF TABLES

LIST OF FIGURES

CHAPTER 1

INTRODUCTION

The problem of target recognition from the scattered electromagnetic fields of targets have long been very difficult to solve, not only because scattering mechanisms are very complicated even for geometrically simple targets, but also due to the fact that these scattered signals are strongly dependent on the frequency, polarization and the aspect angle of the transmitted and received signals.

In particular, aspect dependency of the scattered signals makes the problem more complicated than the other parameters. In general, aspect dependency causes two types of error in classification problems. First, the scattered responses at two different aspects of same target can be incorrectly identified as two different targets. Secondly, the scattered responses of two different targets at different aspects can be incorrectly identified as the same target. Therefore, minimizing the aspect sensitivity of the recognition problem must be a purpose in the design of the electromagnetic target classifiers. A feature extraction technique such that extracted features are minimally sensitive to aspect variations, is needed to accurately characterize targets.

The feature extraction technique used in target classification must possess two critical properties. One of them as mentioned before is to minimize the aspect dependency. The features extracted from the scattered signals of a given target must have low aspect sensitivity, so that signals scattered from the same target at different angles can be closely matched with each other. The second property is that the extracted features must be highly sensitive to geometrical (size, shape) and physical (material composition) properties of the target in concern to discriminate the target

from the other similar targets [1, 2]. For a good classifier, these two properties must be accomplished simultaneously.

Many different target classification techniques such as the techniques based on the use of natural scattered response of a target [3-6], Neural Network (NN) analysis based techniques [7-12], time-frequency analysis based techniques etc, have been proposed in literature. In particular, the use of neural network (NN) based feature extraction techniques in target identification, has been a popular approach in recent years. NN type of feature extraction techniques needs a large set of scattering data at many different aspects for each target to train the classifier. Using such a large database, may not be feasible in most cases. Furthermore, to add a new target or even a new reference angle to a NN type of classifier requires training the whole structure of classifier again with this new reference database [1]. Therefore, to construct a classifier that satisfies the requirements of computational efficiency and adaptability to changing needs, in addition to other design criteria, we have not used a NN type approach in this thesis.

The feature extraction technique used in this thesis, is mainly based on the natural resonance response of targets. The complex natural resonance mechanism in linear time-invariant system models of targets was formalized as the singularity expansion method (SEM) by Baum [13, 14]. When a target is modeled by a linear time-invariant system, target response in the resonance region shows significant damped oscillations due to the zeros of the denominator (simply the poles) of the transfer function of the target. These target poles are called the complex natural resonant (CNR) frequencies of the target. The shape, size and material properties of a target, determine the values of CNR frequencies in an aspect-independent manner. Therefore, the target can be uniquely characterized by the complete set of its system poles.

Although the complete set of CNR frequencies of a target uniquely determines that target in an aspect independent way, the contribution of each pair of CNR frequencies to scattered response depends on the magnitudes of the residues in the transfer function at that frequency. As the angle of incidence and/or reception changes, the set of strongly excited poles (having large residues in transfer function) changes accordingly. Due to this aspect dependency of residues, the scattering data of a target must be obtained from a sufficiently large set of different aspects to capture information about most of the CNR frequencies, so that target classification could be done successfully. This subject will be briefly explained in Chapter 2, where the feature extraction method is introduced.

In this thesis, we have used a set of small-scaled aircraft targets modeled by perfectly conducting, straight, thin wires. When a conducting target is excited by an incident electromagnetic field, it induces currents on the target's conducting surface. When the frequency of the incident wave coincides with the period of oscillation of induced currents, strong resonances will occur [15]. The frequencies at which these resonances occur are CNR frequencies of the conducting body. The effect of these frequencies in the scattered response of a target mainly exists in the late-time period of the scattered response. This period is known to be mainly related to the geometrical features of the target such as its overall shape and size [16]. In early times of the response, the forced and the natural response exists together in an inseparable way. Hence, a feature extraction technique focusing on the natural response like the one used in this thesis, should avoid using the early time portion of the scattered responses.

We will focus on designing an electromagnetic target classifier whose targets are modeled by perfectly conducting, straight, thin wires using a natural resonance based feature extraction technique from target's back scattering impulse responses over only a few different aspects as a reference database. It is aimed that with the feature extraction technique used in this thesis, the designed classifier can discriminate targets with high correct classification rates and also can possess the

properties such as low memory consumption, high detection speed by using a small sized reference database.

The organization of the thesis is as follows:

Chapter 2 describes the natural resonance based feature extraction technique used in this thesis.

In Chapter 3, the process of the generation of back-scattering electromagnetic signals in frequency domain will be discussed with the properties of the simulation program used in that process.

Chapter 4 demonstrates the design of a classifier for a target set of five small-scale aircraft modeled by perfectly conducting, straight, thin wires.

Finally, in Chapter 5, the concluding remarks will be presented.

In Appendix A, some program codes written in FEKO environment to realize the applications in this thesis will be given.

In Appendix B, some program codes written in MATLAB to realize the applications in this thesis will be given.

CHAPTER 2

A NATURAL-RESONANCE BASED FEATURE EXTRACTION TECHNIQUE

2.1. Introduction

In this chapter, we will focus on the natural-resonance based feature extraction technique which is used in this thesis together with its theoretical foundation. As mentioned in the Introduction, a successful feature extraction technique must produce target features with low aspect sensitivity so that signals scattered from the same target at different angles can be closely matched with each other. Secondly, the extracted features must be highly sensitive to geometrical and physical properties of the associated target to be able to discriminate this target from the similar targets. In the resonance region, the most fundamental feature of an electromagnetic target is its set of complex natural resonance (CNR) frequencies (target system poles) whose values are independent of aspects and polarization conditions. These frequencies satisfy those two properties mentioned above simultaneously. In the classifier design technique utilized in this work, we will not use the CNRs directly but use their indirect effects on the late-time region of time-domain scattered signals.

The natural-resonance based feature-extraction method used in this thesis, has been introduced for the first time in literature and applied to a set of dielectric targets by Turhan-Sayan [1, 2], achieving highly accurate results of classification. In this thesis, our aim is to investigate the applicability of this technique to perfectly conducting targets modeled by thin wire structures.

As mentioned earlier, the singularity expansion (SEM) method formalize the complex natural resonance mechanism in linear system models of targets [13, 14]. According to SEM, in the complex frequency domain, the aspect-dependent system function of the target which is modeled as a distributed linear, time-invariant system, can be given as

$$H(s,\Omega) = A(s,\Omega) + \sum_{n=1}^{\infty} \frac{R_n(s,\Omega)}{(s-s_n)(s-s_n^*)} \tag{2.1}$$

where $s = \sigma + jw$ (2.2) with $w = 2\pi f$ (2.3)

The Inverse Laplace transform of this expression can be obtained in the general form,

$$h(t,\Omega) = a(t,\Omega) + \sum_{n=1}^{\infty} b_n(\Omega) e^{-\sigma_n t} \cos(w_n t + \theta_n) \tag{2.4}$$

Obviously, $h(t,\Omega)$ is the aspect dependent impulse response of the target. The symbol Ω represents the aspect dependency in Equations (2.1) and (2.4). And s_n's are the complex-valued system poles occurring in complex conjugate pairs.

The function $a(t,\Omega)$ is needed to represent the forced response stemming from the direct interaction of the excitation (the impulse function) with the target. When the target is of finite size, the function $a(t,\Omega)$ is strictly an early-time contribution lasting as long as the transition time of the excitation over the target.

The damped sinusoidal part is the natural impulse response of the target. The contribution of each target pole s_n to the target response depends on the magnitudes of the residues, R_n's in Equation (2-1). As the aspect of back-scattering changes, the residues of the target poles change accordingly. Therefore, a pole pair which is very

dominant at one aspect may be weakly excited at another aspect contributing to the overall response at a negligible level. On the other hand, a target pole pair leads to a long lasting oscillation in time, if σ_n (the real part of s_n) which is called the attenuation constant (or damping coefficient), is small. For these reasons, the scattering data of a target must be used at a sufficiently large set of different aspects to capture information about most of the dominant CNR frequencies available in late-time portions of each aspect angle's responses. This procedure helps reducing the aspect dependency of the scattered data that complicates the problem of target classification.

To extract target specific information from the target response in the late time region, we can use a joint time-frequency representation. Theoretically, localization of the natural response over the joint time-frequency domain is closely related to the real and imaginary parts of target poles [1]. To avoid the effects of the highly aspect dependent nature of early-time (forced) part of the target's scattered response, the relatively late-time portions of the time-frequency distribution matrices will be used in the feature extraction process.

In this study, the auto Wigner-Ville Distribution (WD) is used as the main signal processing tool for feature extraction to get useful energy related information from the selected late-time portion of the target response signal at every predefined aspect angle. It is a real-valued, quadratic representation, and the original signal's time and frequency spans are preserved. As reported in [17], the WD was found to be more useful than the other time-frequency distributions as it satisfies a large set of desired properties including the important marginal properties. Furthermore, it has been demonstrated by Turhan-Sayan in [1] that late-time feature vectors obtained by using this WD based technique, was found considerably less sensitive to aspect variations as compared to the corresponding time-domain scattered signals for spherical dielectric structures.

The extracted WD based late-time feature vectors, still show considerable amount of aspect dependency. To further reduce aspect dependency, principal

component analysis (PCA) is used for obtaining a single characteristic feature vector for each target from the late-time feature vectors at the reference aspects. The resulting feature vector can effectively represent the target over a broad range of aspects.

The main steps of the WD and PCA based feature extraction technique will be described in the following sections of this chapter.

2.2. Obtaining time domain responses

As it will be demonstrated in Chapter 3, we can obtain the scattered signals for any arbitrary shaped targets in frequency domain. Since we work on time domain responses, we must transform data in hand into time-domain. This process was accomplished in MATLAB environment by using its Inverse Fast Fourier Transformation (IFFT) tools.

If we perform transformation process directly on the frequency responses without windowing, the obtained string in time domain will carry strong numerical noisy components so called Gibbs's phenomena because of the sharp discontinuity at the maximum frequency end of the low-pass data. For this reason, we first perform windowing operation on the frequency responses. The gaussian windowing is chosen for its smooth, continuous nature. The effect of windowing operation on frequency response is illustrated by the example which will be used in Chapter 3 that is 12 m long, perfectly conducting, thin wire. The time output has a total time span of 1 μ sec with 256 sample point. Unwindowed time domain impulse response obtained by IFFT operation is in Fig 2.1.

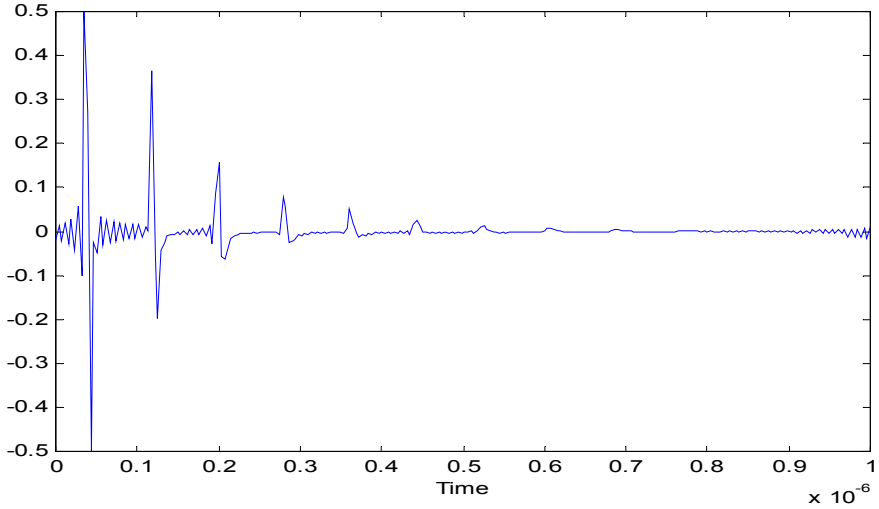

Figure 2.1 12m long wire, unwindowed back-scattered impulse response

In Fig 2.1, the impulse response has Gibbs's phenomena which is the case we don't want at all. This unwanted condition is cleared by windowing the frequency response with a gaussian window which drops to %1 of its maximum value at 120MHz as shown in Figure 2.2.

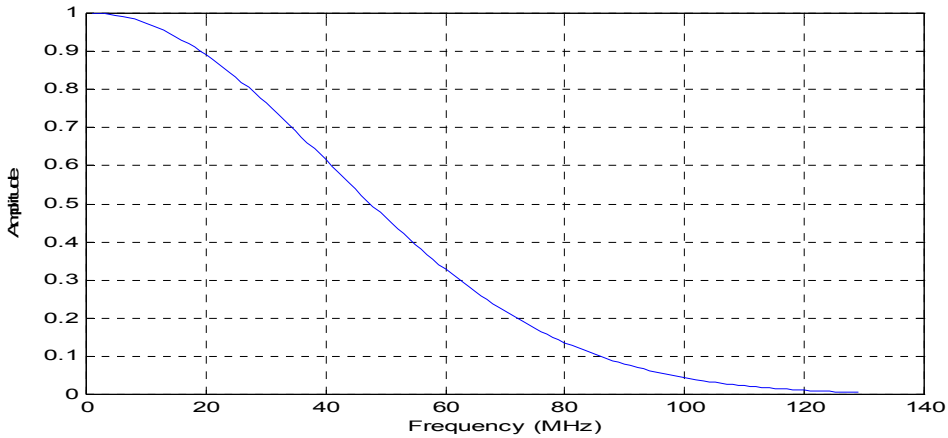

Figure 2.2 The Gaussian Window used to eliminate Gibbs's phenomena

After windowing using the gaussian window shown in Figure 2.2 and performing IFFT operation, the resulting impulse response is given by Figure 2.3. In that figure, we can easily see that Gibbs's phenomena that deteriorate the original signal are removed. Both signals are normalized such that the total energy of each signal equals to unity for a fair comparison.

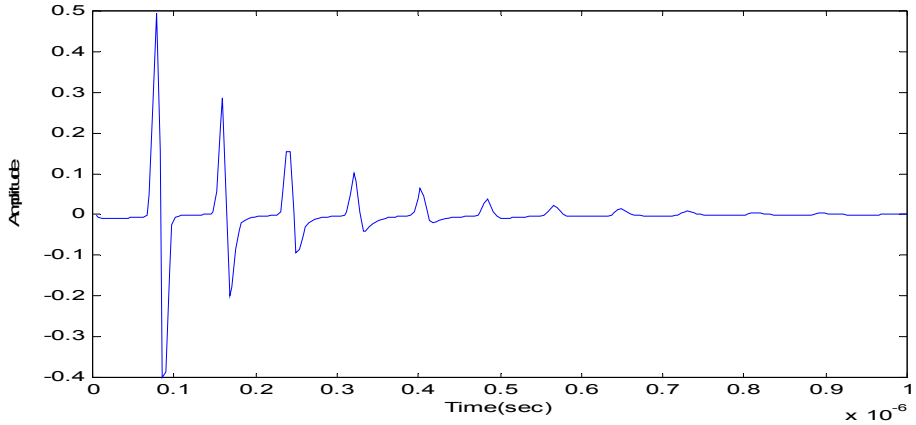

Figure 2.3 12m long wire, Gaussian windowed back-scattered impulse response

2.3. The usage of WD in feature extraction process

As indicated in previous sections, the auto WD is used in the feature extraction method for obtaining target specific features from scattered signals. The reasons for selecting for this time-frequency representation were explained in Section 2.1. But two of them are demonstrated here due to their importance. In a classification problem, extracting features from scattered signals using a common time and frequency intervals for all members of target set and for all aspects is very important for the purpose of a fair comparison. Hence, an important reason for selecting WD among the others is its nature of preserving time and frequency spans of the original signal. To demonstrate, a signal x(t) is chosen as shown in Fig.2.4. This signal has a frequency of 20MHz in time interval of [0.2, 0.4] μ sec and frequency of 50 MHz in time interval of [0.8,0.9] μ sec. The auto WD of this signal is shown in Fig.2.5. As x(t) is real, its WD output has an even symmetry with respect to the frequency. As seen in this figure, the time and frequency spans of original signal x(t) has been preserved and there are lots of interference terms in both time and frequency. Their reasons will be explained later in this section.

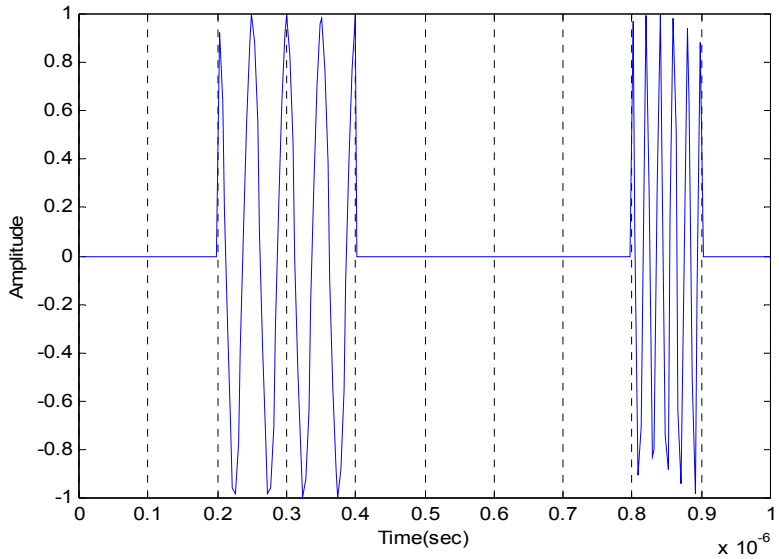

Figure 2.4 x(t), different frequencies in different time-spans

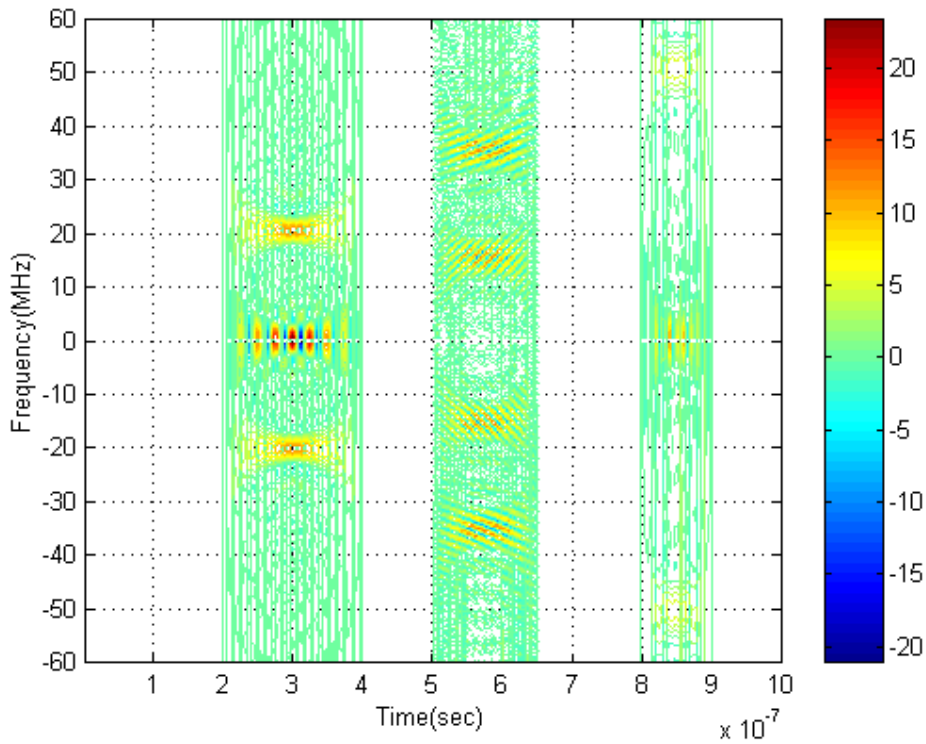

Figure 2.5 The auto-WD of the signal shown in Figure 2.4

In this thesis, for all the signals used in examples, their energies will be normalized to unity for the sake of fair comparison. The time-frequency analysis of these normalized signals will be done by evaluating the auto WD of each signal. The auto WD of a time signal $x(t)$ is defined as,

$$W_x(t, f) = \int_{\tau} x(t + \frac{\tau}{2}) x^*(t - \frac{\tau}{2}) e^{-j2\pi f\tau} d\tau \qquad (2.5)$$

where the superscript (*) means complex conjugate operation. There are marginal properties [18] which WD satisfies. These are given in Equations (2.6) and (2.7)

$$\int_f W_x(t, f) df = p_x(t) = |x(t)|^2 \qquad (2.6)$$

$$\int_t W_x(t, f)dt = P_x(f) = |X(f)|^2 \tag{2.7}$$

where $p_x(t)$ and $P_x(f)$ denotes the instantaneous power and the spectral energy density of the signal, respectively.

By means of satisfying these marginal properties, the WD can be approximately regarded as a two-dimensional distribution of signal energy over the joint time-frequency plane. This is the second reason of choosing WD. This property provides us detection of time intervals on which the most valuable information lies as will be explained in the next section.

Unfortunately, satisfaction of marginal properties do not warrant the interpretation of WD as a time-frequency energy density at every point in the time-frequency plane as explained by uncertainty principle [19] which does not allow infinite resolution in both time and frequency simultaneously [20]. It is also known that WD outputs have very strong and highly oscillatory interference terms that may seriously deteriorate the identification capability of the classifier [2] as seen clearly in Figure 2.5. The WD output may locally has negative values due to interference terms in joint time-frequency plane which contradicts with the physical fact that no negative energy exists in real world. This contradiction can be explained by uncertainty principle. As reported in [1], getting rid of such unwanted negative entries by replacing the negative entries by zeros in WD matrix during the feature extraction process, improves the classification performance remarkably. To demonstrate, the signal in Figure 2.3 is taken into consideration again. In Figure 2.6, the original auto WD of the impulse response signal of Fig 2.3 is shown. To be able to show the negative-valued interference terms a colorbar is given nearby the figure. It is easily seen that the blue colored points on the graph, represent negative valued WD outputs which does not coincide with the physical expectations. Also, in Figure 2.7, the auto WD of the same signal is constructed by taking only its non-negative entries by using the formula in Equation (2.8). In both figures, only the half of the

frequency axis is shown corresponding to positive frequency region due to symmetric nature of WD matrix with respect to frequency.

$$W_x(t, f) = \frac{W_x(t, f) + abs(W_x(t, f))}{2} \tag{2.8}$$

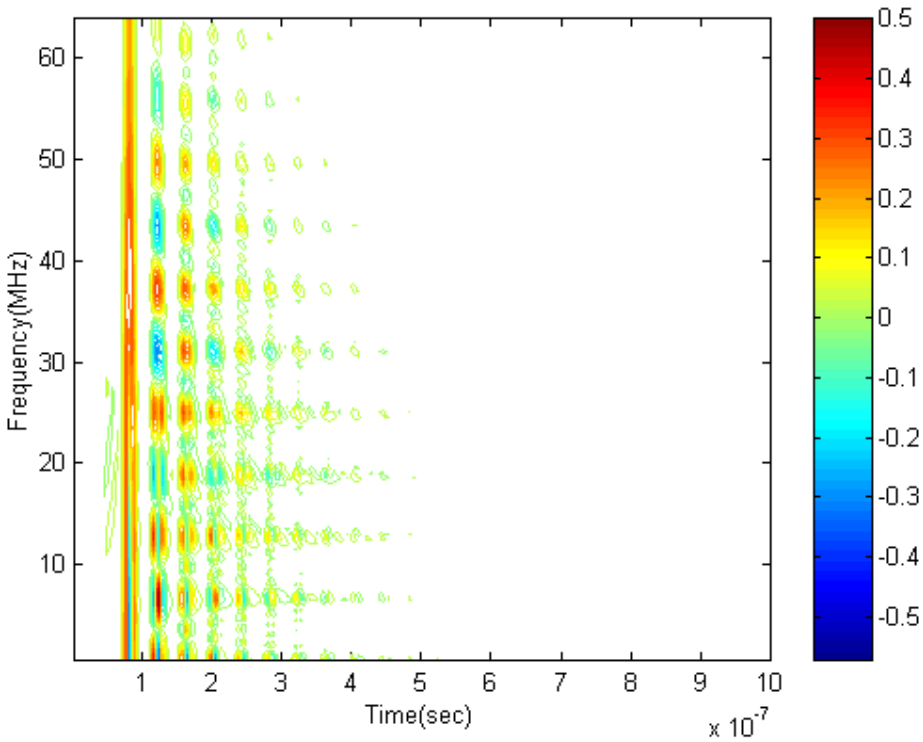

Figure 2.6 The auto-WD of the signal shown in Figure 2.3

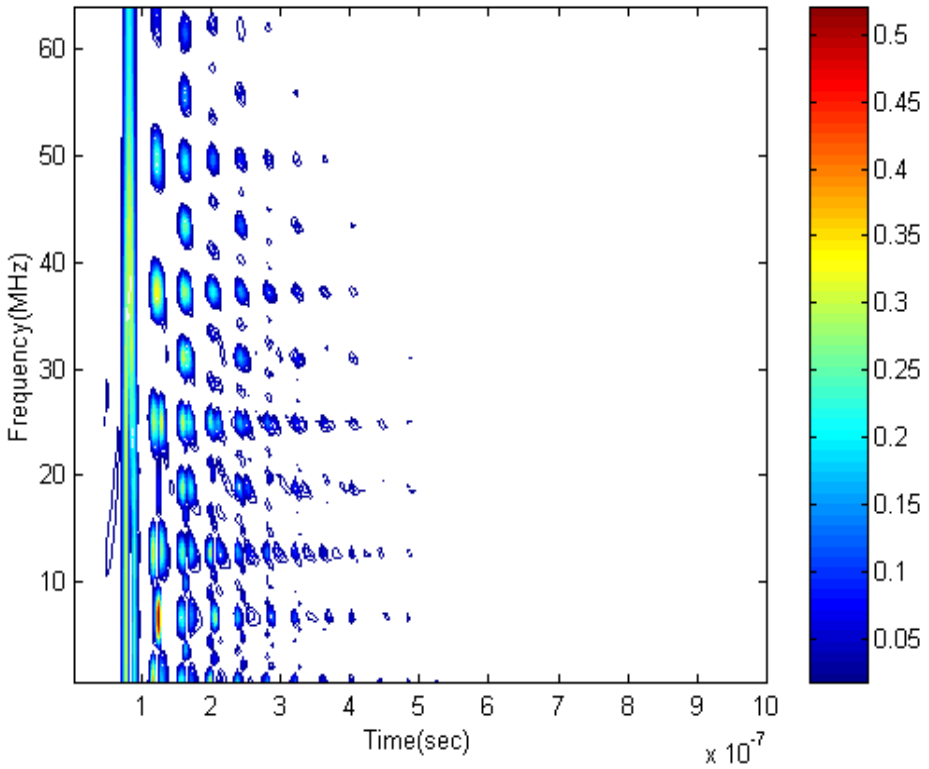

Figure 2.7 The non-negative auto-WD of the signal shown in Figure 2.3

It is seen in Figure 2.7 that all negative entries has been removed. In the rest of this thesis, we will use non-negative auto WD computation in signal processing. Also, only the non-negative frequency region of WD matrix will be used in the rest part of this thesis since, due to symmetry, both negative and positive frequency regions contain the same information.

2.4. Construction of late-time feature vectors

Even after making the operations explained in the previous section, the resulting WD output may not be found to be useful enough to be used in target classification. WD output in hand needs to be further processed to get late-time feature vectors used to find best time interval in which the distribution of natural resonant frequencies could be found in the most discriminative manner.

For a normalized scattered signal, x(t), from a predefined aspect angle for any target in the target set of classification, the output auto WD matrix of x(t), has a size of (N x N) where N is the length or in other words total number of time samples of discrete time-domain signal x(t). Since, for all real-valued signals, the WD output matrix has even symmetry with respect to frequency, it is enough to process on the non-negative frequency portion of WD matrix which has a size of (N/2 x N). The total time span T_0, is then divided into Q time intervals that have equal length of T_0/Q seconds. By means of one of the marginal properties which is given by Equation (2.7), the amount of energy contributed to each sub-interval q by a spectral component f_m is given by [1].

$$E_q(f_m) = \int_{(q-1)\Delta}^{q\Delta} W_x(t, f_m)dt \qquad \text{for q=1,2,3,.....Q} \qquad (2.9)$$

where $\Delta = T_0/\text{Q}$, m =1,2,....,N/2 and $f_m = (m-1)/(2T_0)$.

Energies supplied by each spectral component f_m into q th subinterval, can be put into a vector form,

$$\overline{E}_q = [E_q(f_1) \quad E_q(f_2) \ ..... E_q(f_{N/2})] \qquad (2.10)$$

Since there are Q bands at all, the so called partitioned energy density vector $\overline{E}$ is given as a combined form of Equation (2.10) for each subinterval q;

$$\overline{E} = [\overline{E}_1 \quad \overline{E}_2 \ ..... \overline{E}_Q] \qquad (2.11)$$

which has the length of Q x N/2. This operation was performed on total time span. As explained before, we want to catch natural resonance components that appear in late-time region of data. Therefore, it is possible to choose a few successive partitions of $\overline{E}$ in late time region to construct the corresponding late-time feature vector (LTFV). Taking at least two successive time intervals in feature vector construction is necessary to capture some indirect information about the real parts of the natural resonance frequencies as they control the rate of attenuation of the natural response. By selecting two successive partitions of $\overline{E}$, corresponding to indices q^* and q^*+1, target characterization capability of the classifier can be improved significantly as reported in [2]. Then, the total length of the extracted late-time feature vector, becomes 2 x N/2 = N which is the length of the original signal x(t). Hence we end up with reduced aspect sensitivity, reduced dimensionality and significant gain from computational time required for real time decision. Indeed, with smaller aspect sensitivity of LTFVs, we need only scattering signals from only a few aspects for each member target to construct the reference database of the classifier.

It is important to select Q value which determines how many subintervals that total time span T_0 would be divided into. As Q value changes, the time span associated with each sub-interval q changes also. Since, we will only focus on a few sub-intervals in the late-time region, total time span chosen to be analyzed, depends on both the value Q and the selected sub-intervals in the late-time region. Therefore, it is critical to select the optimum values of Q and q^* for catching the natural resonance components of the scattered responses in LTFVs which will be used to construct the reference database of the classifier. Once Q and q^* is determined at the design step, they must be kept fixed since the same values must also be used for the test signals in decision-making step. In the next section, the procedure for determining these design parameters automatically will be briefly explained.

2.5. Determining design parameters of the classifier

To construct the reference database of the classifier, we need to obtain a LTFV for each predefined reference aspects of each target. Getting them in hand, enables us to reduce aspect sensitivity of the classifier. This reduced aspect sensitivity also provides us an option to construct a reference database from LTFVs created by scattered signals for only a few aspects as explained in previous sections.

In construction process of LTFVs, selecting the parameters Q and q*, plays an important role on the accuracy performance of the classifier. They are chosen by using scattered data only at the reference aspects. The algorithms used for this purpose, must be independent from the type of the targets to be classified [2]. We will not go into details of the programs developed for selecting the optimum values of Q and q* in MATLAB environment. But the main ideas behind them will be explained here.

Because of using scattered data that has a length of a power of two for computational efficiency in programming, the range of Q values in which the optimum Q is selected, is chosen from the powers of two also like a set of [8, 16, 32]. Then, for each value of Q in the set, the procedure is as follows;

Step 1. First of all, for a given target, partitioned energy density vectors defined on full time span ($\overline{E}$'s which is given by Equation(2.11)), are constructed for each of scattered data for all M predefined reference aspects. Then, one of $\overline{E}$ associated with one reference aspect, is chosen among them and correlation coefficients between this vector and the other M-1 ones associated with other reference aspects, are calculated.

Step 2. The procedure explained in step 1, will be repeated for the other candidate targets. Hence after this step, each target's the correlation coefficients graphs between partitioned energy density vectors of reference aspects, was

obtained. Then for each graph, variance of them is computed and stored as measure of aspect dependency. To clarify, let us assume that we have K targets, then we have a variance vector of length K.

Step 3. Step1 and 2 will be repeated for the other values of Q in the set.

Step 4. Finally, we have variance sequences for each value of Q in the set. The value at the Kth member of each sequences denote aspect dependency of reference aspects for K^{th} target. We want these values to be as small as possible to determine the best value of Q that provides the smallest aspect dependency. Therefore, all the variance sequences associated with each value of Q are plotted on same graph, and the Q value that corresponds to the smallest values for each target, is chosen as the optimum Q value. This process will be demonstrated in Chapter 4, with the target set constructed for small-scale aircraft structures modeled by perfectly conducting wires.

Once we determine the optimum value of Q, we know that the total time span T_0 should be divided into Q equal length sub-intervals. The next thing to do is to determine which sub-interval gives the best classification performance.

Another program is developed in MATLAB to select the optimum value of q*, which determines LTFV $\overline{e}$ from Equation (2.11) as

$$\overline{e} = [\,\overline{E}_{q*} \quad \overline{E}_{q*+1}\,] \tag{2.12}$$

As we are still in the process of classifier design, we use only the reference data scattered from predefined aspects again. The procedure for determination the value of q* is based on the concept of Correct Classification Factor (CCF) introduced in [2]. By computing CCF which is given by Equation (2.13) below,

$$CCF\ (q^*) = \frac{1}{KM^2}\sum_{i,j} r_{i,j}^{matched} - \frac{1}{(K^2-K)M^2}\sum_{i,j} r_{i,j}^{mismatched} \tag{2.13}$$

we can detect the optimum value of q* at which CCF is maximum. In Equation (2.13), K is the number of targets and M is the number of reference aspects. Also, $r_{i,j}^{matched}$ is the correlation coefficient between any two LTFVs which belong to the same target at different aspects. Similarly, $r_{i,j}^{mismatched}$ is the correlation coefficient between any two LTFVs which belong to different targets. Since, the correlation coefficient between two vectors represents the similarity between them; we expect high values for matched correlation coefficients and low values for mismatched correlation coefficients if the classifier design is a good one.

For each value of q* ranging from 1 to Q-1 (for using two successive time intervals), correlation coefficients between LTFVs constructed from the time span of [q* and q* +1], are computed for all M reference aspects and for all K targets. Let us assume we have three targets to be classified and we have reference data for five aspects for each target. So, K=3 and M=5 and the resulting number of LTFVs is K x M = 15. The resulting correlation coefficient table between these LTFVs has a size 15 x 15 =225. Since we have 3 target at all, there is K X K =9 blocks on the correlation coefficients table, each has a size M x M =25. Among these blocks, three (K) of them denotes the matched regions for each target and the other six ($K^2 - K$) denotes the mismatched regions. The sums of correlation coefficients resulting from matched and mismatched regions are calculated separately and then normalized by dividing them to the size of each region. Finally, the difference between the normalized sum of matched regions and that of mismatched regions are computed and stored as the CCF for this q*. The whole process is then repeated for each q*. The q* that has the maximum CCF value is then taken as the optimum value of q*. Therefore, the LTFVs are constructed by using Equation (2.12) for this optimum q*.

The determined Q and q* values are classifier design parameters. The reference database of LTFVs will then be constructed by using these values. Therefore, they must be kept fixed during the processing of test signals also for proper comparison. The procedure described in this section so far, will be applied to the classification example in Chapter 4.

2.6. Usage of PCA on extracted features

Up to now, we have described how to select our design parameters and construct LTFVs for all reference aspects of all targets. For the sake of integrity, again assuming that we have K targets and M reference aspects, the total number of LTFVs will be K x M. These LTFVs will be used later in the test of the classifier. A target and an arbitrary aspect different from reference aspects will be chosen and then the LTFV of this data will be created. Next, the correlation coefficients between this LTFV and those of reference aspects will be computed. Decision can be made by choosing the target associated with the LTFV among (K x M) LTFVs, which has the highest correlation coefficient with the test LTFV. So, for the case of three targets and five reference angle, we need to compute correlation coefficients between LTFV data and 15 reference LTFVs. This may take computational time which may not be sufficiently short for real-time identification. To reduce the computational time by decreasing dimensionality and to increase the classification accuracy due to the multi-aspect fusion of feature vectors, we will use Principal Component Analysis (PCA).

PCA is a well-known statistical method which was first introduced by Pearson in 1901 [21] and has been widely used in different scientific areas of data analysis and compression, dimensionality reduction and feature extraction in recent years. The PCA technique has been applied to electromagnetic target classification problems [7, 22], but so far, this usage was limited to the purpose of reducing dimensionality of feature vectors at each specified aspect of a given target. In this thesis, however, we will use the PCA technique for multi-aspect feature fusion as introduced by Turhan-Sayan in [2].

By means of using PCA, for a given target, LTFVs of all reference aspects can be integrated into a single vector named ‘fused feature vector’ (FFV). Therefore, test process can be done by comparing test LTFV with only FFVs of each target.

Hence, dimensionality and consequently computational time is reduced by a factor of number of reference aspects M. In fact, aspect sensitivities of resulting FFVs are much smaller than those of LTFVs as will be illustrated later. Therefore, a more important reason of using PCA in this thesis, is that by applying PCA on LTFVs for all reference aspects of a target, the resulted FFV of the target can represent that target in an almost aspect independent manner. This property improves accuracy performance of the classifier.

Since PCA is individually a very wide concept in theoretical sense, its mathematical derivation is not given here. But, the application of PCA to our case is demonstrated. For integrity, again assuming that we have M reference aspects, and N is the length of each corresponding LTFVs. And F is feature matrix of size M x N whose rows are LTFVs Equation (2-12) of a given target at M reference aspect.

$$F^{T} = [\,\overline{e}_1^{T} \quad \overline{e}_2^{T} \;\ldots\ldots\ldots\ldots\; \overline{e}_M^{T}\,] \tag{2.14}$$

where T denotes the transpose operator.

The covariance matrix S_F of the feature vector F, is a symmetric matrix (of size M x M) is given in Equation (2-15);

$$S_F = \begin{bmatrix} s_1^{\,2} & s_{12} & \ldots & s_{1M} \\ s_{21} & s_2^{\,2} & \ldots & s_{2M} \\ . & . & & . \\ . & . & & . \\ . & . & & . \\ s_{M1} & s_{M2} & \ldots & s_M^{\,2} \end{bmatrix} \tag{2.15}$$

where its off-diagonal entries s_{ij} denote covariance between LTFVs $\overline{e}_i$ and $\overline{e}_j$, and the diagonal entries s_i^2 represents the variance of LTFV $\overline{e}_i$.

The covariance matrix S_F can be transformed into a diagonal matrix Λ by means of similarity transformation;

$$\Lambda = U^T S_F U \quad = \begin{bmatrix} \lambda_1 & 0 & \dots & 0 \\ 0 & \lambda_2 & \dots & 0 \\ . & . & & . \\ . & . & & . \\ . & . & & . \\ 0 & 0 & \dots & \lambda_M \end{bmatrix} \tag{2.16}$$

where U is the modal matrix in the form of

$$U \ = [u_1 \quad u_2 \dots\dots\dots u_M \ ] \tag{2.17}$$

with u_i 's being the normalized eigenvectors corresponding to eigenvalues of the covariance matrix S_F . The eigenvalues λ_i are then solved from

$$\det(\ S_F \ - \ \lambda I \ ) \ = \ 0 \tag{2.18}$$

where I is the identity matrix of size M x M. Then, λ_i (eigenvalues) are ordered from the highest to the lowest. The corresponding eigenvectors t_i are solved from

$$[S_F \ - \ \lambda_i I \ ] t_i \ = \ 0 \qquad \text{i =1, 2,.....M} \tag{2.19}$$

These orthogonal eigenvectors are normalized for obtaining the orthonormal eigenvectors,

$$u_i \ = \ \frac{t_i}{\sqrt{t_i t_i^T}} = \frac{t_i}{|t_i|} \tag{2.20}$$

to construct the matrix U that is used to transform the correlated LTFVs of into a set of uncorrelated vectors, z_i for i=1,2, ...M

$$Z = \begin{bmatrix} z_1 \\ z_2 \\ \text{M} \\ z_M \end{bmatrix} = U^T \begin{bmatrix} \overline{e}_1 - mean\ (\overline{e}_1) I_N \\ \overline{e}_2 - mean\ (\overline{e}_2) I_N \\ \text{M} \\ \overline{e}_M - mean\ (\overline{e}_M) I_N \end{bmatrix} \tag{2.21}$$

where I_N is a unity row vector of length N and the resulting Z matrix has a size of M x N same size with feature matrix F. z_i 's are called the principal components of feature matrix F. Each z_i vector has zero-mean, and variance of λ_i. The first principal component of feature matrix F, that is z_1, has the highest correlation coefficients with LTFVs $\overline{e}_i$ since λ_1 has the highest percentage in the summation of λ_i for i=1,2,.....,M [21]. Therefore, z_1 the first principal component can be regarded as the fused feature vector (FFV) of target by itself neglecting the other principal components of z_2, z_3 ,.... z_M , if λ_1 is much larger than the rest of the eigenvalues.

If desired or required, the other principal components can be linearly combined to construct the FFV of the target by proper weighting factors ($\overline{\lambda}_i$) as described in Equation (2.22) below,

$$FFV = \sum_{i=1}^{M} \overline{\lambda}_i z_i \qquad \text{where} \qquad \overline{\lambda}_i = \frac{\lambda_i}{\sum_{i=1}^{M} \lambda_i} \tag{2.22}$$

Obviously, a weighting factor $\overline{\lambda}_i$ gives the ratio of the variance of the ith principal component to the total variance of the data.

CHAPTER 3

GENERATION OF SCATTERING RESPONSES

3.1. Introduction

The scattered responses of a target in time-domain can be obtained either from direct measurements or by solving an integral equation in the time-domain (TDIE) or by some other time-domain techniques such as the Finite Difference Time Domain (FDTD) approach [23]. While such direct time-domain algorithms are excellent tools for the analysis of scattering response from general two-dimensional target, they are computationally intensive for the three-dimensional problem of interest [24]. Thus, the back-scattered signal database used in the classifier design for wire structures of this thesis, is numerically generated in the frequency domain. Then, the corresponding time domain back-scattered signals are obtained by using Inverse Fast Fourier Transform (IFFT) procedure together with proper windowing.

To compute the scattering responses of the targets in frequency domain, we have used a simulation program named FEKO that is an abbreviation derived from the German phrase **Fe***ldberechnung bei* **K***¨orpern mit beliebiger* **O***ber.¨ache.* (*Field computations involving bodies of arbitrary shape.*) As the name suggests, FEKO can be used for various types of electromagnetic field analyses involving objects of arbitrary shapes such as near and far field analyses.

Different excitation strategies are available in FEKO such as the plane wave excitation, gap voltage formulations, ring currents, impressed currents, etc. For the applications in this thesis, we have used only the plane wave excitation format as the incident field.

In the FEKO simulation software program, many small linear segments or triangular patches depending on the geometry, are used to form a target. The current distribution on the conducting surface of a target is then obtained by calculating current distribution on each of the small patch.

The program FEKO is based on the *Method of Moments* (MoM). Electromagnetic fields are obtained by first calculating the electric surface currents on conducting surfaces, (which is our case because of we will only use perfectly conducting, thin wire structures throughout this thesis) and equivalent electric and magnetic surface currents on the surface of a dielectric solid. FEKO implements the frequency-domain MoM solution of the Electric Field Integral Equation (EFIE) for low frequencies problem, and the Physical Optics (PO), Geometrical Theory of Diffraction (GTD) and Uniform Theory of Diffraction (UTD) for high frequencies problem. The currents are calculated using a linear combination of basis functions, where the coefficients are obtained by solving a system of linear equations. Once the current distribution is known, further parameters can be obtained e.g. the near field, the far field, radar cross sections, directivity or the input impedance of antennas [25, 26].

WinFEKO is the main user interface module. It is used to control the solution of a problem (e.g. calculating the far-field of a target). The geometry or target is first defined in terms of high level commands in an input file (*.pre) which also sets the solution parameters. User can edit and create the input file by using the customized text-editor named EditFEKO. EditFEKO also enables user to create any arbitrary geometry. The pre-processor PREFEKO then processes this file and prepare the input file (*.fek) for the program FEKO which is the actual field calculation code.

Since, in this thesis we only use perfectly conducting, thin wire structures to construct the target sets, we need to write relatively simple codes in EditFEKO editorial module. Some of the codes written for target set used in Chapter 4 are given in Appendix B. In Figure 3.1, for 12 meters long, straight thin wire (with length to radius ratio is 2000) lied on x axis symmetrical to origin, the magnitude of the back-

scattering frequency response obtained from FEKO is given. Incident plane wave is constructed as the propagation vector towards to origin, is on the line determined by theta=90 and phi=30 degrees and frequency range of concern is 1 to 128 MHz with the frequency step of 1MHz. We can easily see CNR frequencies, and verify the first natural resonance frequency with a simple calculation. For the first complete travel of surface current on the wire, the required length 2L= 24m, the corresponding frequency is c/2L=12.5MHz, where c is the speed of light. The result is approximately same with the one in the figure. The first CNR is viewed as 12MHz in figure because of our frequency resolution is 1MHz.

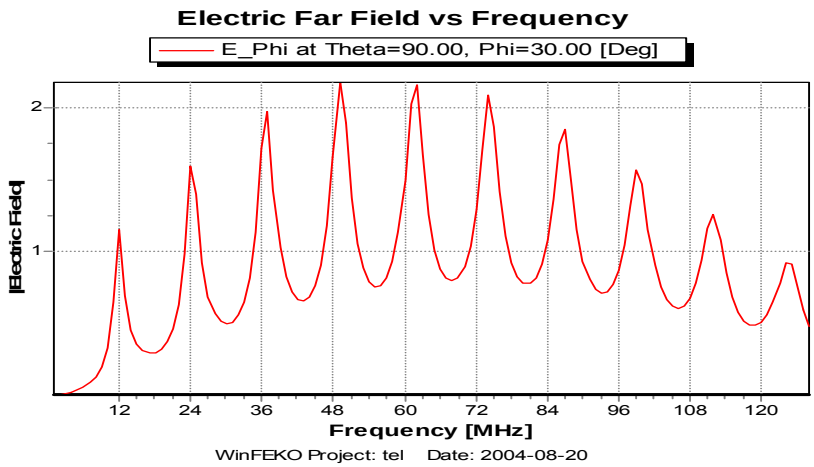

Figure 3.1 12m long wire, the magnitude of back-scattered electric far field frequency response

We will not go into details of the usage of all of the commands in the command list of the program. But, there are some important commands that are critical for obtaining sufficiently accurate results from the program. These are entering the geometry of structure with the segmentation rules which affects the flow of current on the conducting surface of wires and the accuracy of far field response calculations, defining the frequency range of concern, the details of giving incident plane wave properties to the program and using special output format.

3.2. The geometry of the structure

Since in this thesis, we will use target types that are modeled by perfectly conducting structures, the codes for creating geometry required for the simulation is relatively simple. In all cases whatever the target type is, the geometry is first entered by defining points and then constructing the structure in terms of these points. To do this, first two commands must be used named DP and BL cards. DP command is used for defining points and BL command is used for to construct a wire between two points which was previously defined by DP commands. The codes used to obtain the back-scattering response for the 12m wire whose frequency response was given in Figure 3.1 are as follows;

```
#dlen=12
DP   bas    -#dlen/2  0    0
DP   son     #dlen/2   0   0
BL   bas  son
```

In DP command, bas and son are the names of points or the nodes and the others are the Cartesian coordinate system parameters (x, y, z). And BL command is used to construct wire. So the resulting structure is wire between points (-6, 0, 0) to (6, 0, 0).

As stated before, FEKO uses many small segments to construct straight structures. The accuracy of the far-field calculation will increase, if the number of segments is increased [25]. This can be achieved by decreasing the maximum segment length. The constraint in FEKO for maximum segment length is that, it must be smaller than one tenth of minimum free space wavelength of the incident signal to obtain sufficient number of segments for accuracy [26]. In all simulation codes which are used for examples that will be given in Chapter 4, maximum segment length is always chosen as 1/20 of minimum wavelength of incident field.

The other restriction is about wire radius. Segment currents must only flow in the axial direction of the wire to simulate thin wire structures. Since we must avoid

surface currents flowing at circumference of the wire, segment length should not be too short relative to the wire radius. Statement for that is any segment length should be at least 4 times of the wire radius [25]. In all simulation codes written in FEKO to be used in this thesis, this constraint is always checked. For wire radius another command is used named IP command. This command sets the maximum segment length and wire radius simultaneously. Again, for the example of 12m wire, the codes are as follows together with their explanations,

```
#fmin=1e6
#fmax=128*#fmin          ##The first two lines sets the frequency range
#lammin=#c0/#fmax        ##Calculates the minimum wavelength in free-space
#dlen=12                 ## Wire length is 12m
#seg=#lammin/20          ## maximum segment length rule
#rad=#dlen/2000          ## setting wire radius as 6mm
#check=#seg/#rad         ## checking second constraint
!!   if #check<4  then
EN
!!endif
IP    #rad    #seg       ## wire radius and maximum segment length is entered to program.
```

3.3. Defining the frequency range

Another important property is selecting frequency range of incident plane wave. It is easy to estimate the frequency range since we are focusing on simple thin, perfectly conducting structures. As shown in Figure 3.1, sufficient number of CNR frequencies is enabled for a target of 12m thin wire in the frequency range of 1MHz to 128 MHz with 1MHz step size. In this thesis, we always try to use sample number as a power of 2, because it enables us an easy transformation from frequency to time domain. Of course, while classifying a target set, dimensions and geometric structures of all targets in that set, should be taken into account to obtain a discriminative set of CNR frequencies.

In FEKO, discrete frequency set is used to obtain frequency response. To declare the frequency range, FR command that is used for the example of 12m wire, is shown below,

```
#fmin=1e6
FR   128  0              #fmin     #fmin
```

128 is the number of frequency samples used, ‘0’ parameter means we are using linear scaling. The other parameters identify starting frequency and the frequency increment in Hz respectively. In our case, both of them is 1MHz.

3.4. Entering the incident plane wave parameters

While using the program FEKO, it is critical to properly define the excitation (the incident plane wave in our case) for the given target geometry. This is achieved by A0 command in EditFEKO. This command enables us to create an excitation by a linearly polarized incident plane wave. In Figure 3.2, the geometric structure which is used to supply an incident plane wave is shown. Target is assumed to be located at the origin.

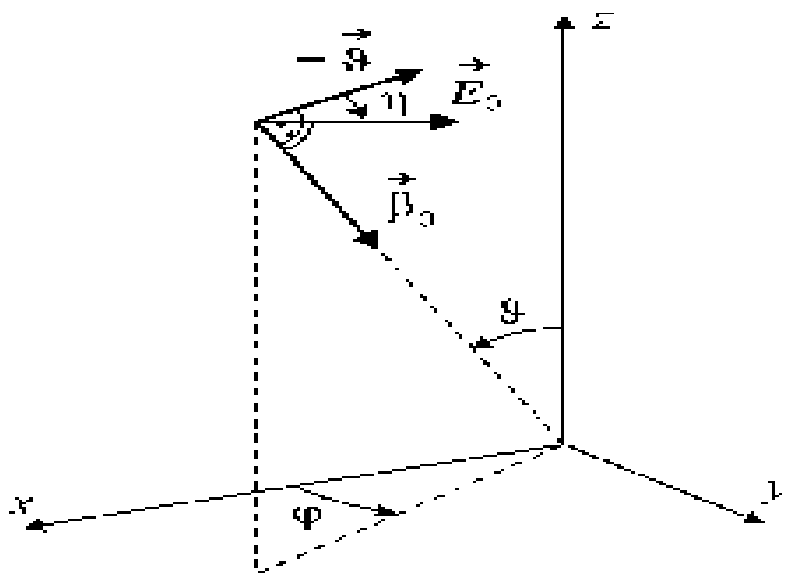

Figure 3.2 Direction of propagation β_0 and direction of polarization η of the incident field [25]

The direction of propagation β_0 is specified by incidence angles ϑ and φ. The polarization angle η (measured from the negative of the spherical coordinate system unit vector $\hat{\vartheta}$ to the field strength vector E0) is defined as indicated in Figure 3.2.

There are some parameters used in AO command. These are;

ANFL 0: New excitation, replaces all previous excitations.
1: Additional excitation, add to previous excitations

In this thesis, we always use 0 for this parameter choice in order to obtain each aspect angle's scattering response separately.

NTHEI If more than one direction of incidence is to be examined; this parameter indicates the number of incident directions points in the ϑ direction. If this field is left empty or a 0 is entered, then NTHEI=1 is set.

NPHII If more than one direction of incidence is to be examined; this parameter indicates the number of incident directions in the φ direction. If this field is left empty or a 0 is entered, then NPHII=1 is set.

For same reason at ANFL parameter, NTHEI and NPHII parameters are always selected as 1.

EIR1 Value of the field strength E0 of the incident field in V/m.Throughout this thesis, we use field strength of 1 V/m.

EIR2 Phase of the field strength E0 of the incident field in degrees. This is not an important parameter hence we choose it as 0 degree

The following parameters are used for the application in Chapter 4 to create back-scattering response of target sets and vary depending on the geometry of concern. Only EIR8 parameter is always selected as 0 to obtain linearly polarized incident plane wave.

EIR3 Angle of incidence ϑ (theta) of the plane wave in degrees

EIR4 Angle of incidence φ (phi) of the plane wave in degrees

EIR5 Polarization angle η in degrees (It is the right- handed rotation viewing in to the incident direction from $-\vartheta$ to the direction of propagation)

DTHEI If more than one direction of incidence is to be examined; this value is the increment in the direction of incidence in the ϑ direction

DPHII If more than one direction of incidence is to be examined; this value is the increment in the direction of incidence in the φ direction

EIR8 Axial ratio v of the polarization ellipse in the range -1 to 1with the following meaning;

v = -1: LHC (left-hand circular) polarized incident wave

-1 <v<0: Elliptical polarization with axial ratio |v|, left-hand rotating.

v = 0: Linear polarization

0 <v<1: Elliptical polarization with axial ratio |v|, right-hand rotating.

v = 1: RHC (right-hand circular) polarized incident wave

In the sense of above instructions, the A0 command code that was used to create Figure 3.1 is given below. The codes are created automatically by the program as soon as the user gives parameters. First 0 means that it is a new excitation source, the following three 1's mean we use only one incident field direction and field strength is 1 V/m. The following 0 is phase of the incident field. ϑ=90 and φ=30 degrees choice means that we are in the x-y plane as could be estimated by Figure.3.2. The last parameter is the polarization angle η is selected as 90 degrees to make E0 lie in x-y plane since - $\hat{\vartheta}$ in Figure 3.2 at this case is +z unit vector.

A0 0 1 1 1 0 90 30 90

3.5. Obtaining Far-field Frequency Response

Since, we look at the targets, in a back-scattering manner, using an observation point at the same aspect angles ϑ and φ of incident excitation field and to avoid near-field interactions; we need far field responses of targets. In FEKO, this is achieved by a command named FF. There are several options for that command like far-field calculations as specified by users, integrate over a specified area and many more. Only the options suitable for this thesis's requirements are explained here. Since, we only want far-field back-scattered response with no interaction with incident field, we set FF card parameters that has meanings

1. Fields calculation only in the incident direction
2. Calculate only the scattered part of the field

For these requirements, the editor of program creates a FF command as 'FF – 2'.

To write the results of far field calculations to an output file to use them later for transforming them to time domain in MATLAB environment, we need another command that is DA command. For the reason of simplicity, only the parameters for writing far-field responses to an output file, is explained here. It must be noted that far field calculations is done in spherical coordinates. Since R is the direction of propagation, only ϑ and φ components of the electric field back-scattering far-field frequency responses are written to a specially formatted output file with a file-name extension 'ffe'. To do this we use a DA command with a parameter DAFFE is set to 1. DA command used for the all program codes written in this thesis is shown below

DA 0 0 1 0 0 0

The zeros in the parameter field represents the other output-file formats like near-field, gain etc. Only parameter DAFFE which writes far-field components of back-scattered electric-field frequency responses is set to 1.

The next thing to do is using this special output file. Since, it has a special format, we open it as an excel file, make necessary regulations and copy columns which include ϑ and φ components of the electric far field response. At last, those excel columns are loaded to a MATLAB file. In our example of 12m thin wire, magnitude of ϑ component of electric field is very small. Hence, we only select φ component of electric field as in Figure 3.1.

CHAPTER 4

CLASSIFICATION OF THE SMALL-SCALE AIRCRAFT

4.1. Introduction

In the previous chapters, computation of scattered responses for wire structures and also the natural resonance based feature extraction technique to be used for extracting target specific features from those scattered signals, were briefly explained. In this chapter, a target classifier will be designed for a target set of five small-scale aircraft which are modeled by perfectly conducting, straight, thin wire structures.

As the first step of this design procedure, scattered frequency responses of these aircraft at various back-scattered aspects are computed by using the simulation software FEKO whose programming structure has been described in Chapter 3. The program codes developed in FEKO environment for obtaining scattered frequency responses of all aircraft targets at desired aspects are given in Appendix A. These frequency domain scattered responses are first windowed and then transformed into time domain by using the IFFT process as mentioned earlier. Next, several reference aspects are chosen for classifier design and the design parameters Q and q* are determined by applying the method explained in Section 2.5. We will then create the LTFVs for each reference signal and construct the FFVs associated with each aircraft target by applying the PCA to LTFVs as illustrated in Section 2.6. Finally, the performance test of the classifier will be carried on with three different criteria.

In this electromagnetic target classifier design, we have selected five aircraft which are Airbus, Boeing 747, Caravelle, P-7 and Tu 154 as the target set. Dimensions of all targets are reduced to one percent of their actual sizes. The resulting wire lengths for the body, wing and tail of each target are given in Table 4.1. It should be emphasized here that the idea of using this target set, is emerged form the usage of same set in reference [7]. In that reference, a completely different target classification method based on Adaptive Gaussian Distribution, PCA and NN is used at 46 reference aspects for each target in the range of [0-90] degrees azimuth angle to train the classifier. One of the purposes of this thesis study has been to show the fact that target classification for this specific target set can be successfully demonstrated by using a much smaller number of reference aspects instead of using a very large number, like 46 used in [7].

Table 4.1 Dimensions of five aircraft targets [7]

Substructures	Target 1 (Airbus)	Target 2 (Boeing 747)	Target 3 (Caravelle)	Target 4 (P-7)	Target 5 (Tu 154)
Body length (m)	0.5408	0.7066	0.3200	0.3435	0.4790
Wing length (m)	0.4484	0.5964	0.3440	0.3250	0.3755
Tail length (m)	0.1126	0.2217	0.1092	0.1573	0.1340

All five aircraft are modeled by perfectly conducting, straight, thin wires (with length to radius ratio is 2000 for all wire structures) as indicated before. The back-scattered responses are obtained from aspects of ϑ=60 degree fixed and φ varies the range of [0-90] at 5, 10, 15, 22.5, 30, 37.5, 45, 52.5, 60, 67.5, 75, 82.5 degrees. Hence we have a total number of twelve different aspects for each target. Only three of them will be used as reference aspects to design the classifier. The rest nine aspects will be used as test aspects to compute the performance of the classifier. The localization of the targets in 3-D geometry, are same with the ones used in [7], as shown in Figure 4.1.

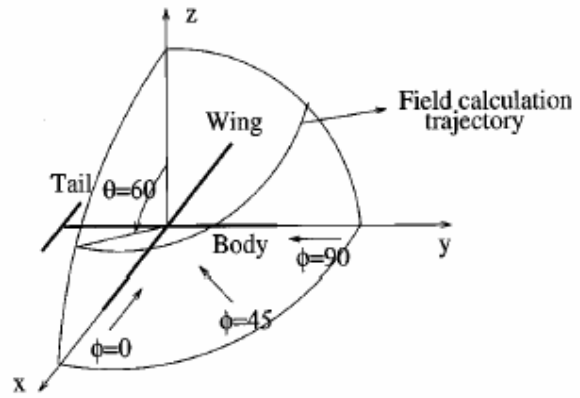

Figure 4.1 Target geometry and the back-scattered field calculation [7]

The back-scattered fields are calculated over the frequency range from 4MHz up to 1024MHz with the frequency step of 4MHz at a total of 256 frequency sample points. For a total of 12 (reference and test) aspects for each one of five targets, the magnitudes of the resulting 60 unwindowed back-scattered frequency responses are plotted on the same frame in Figure 4.2.

The gaussian window used to eliminate Gibbs's phenomena of time domain data due to direct transformation to time domain as demonstrated in Section 2.2, is shown in Figure 4.3, which drops to %1 of its maximum value at 1 GHz. Also, the windowed frequency responses of Figure 4.2 are given in Figure 4.4.

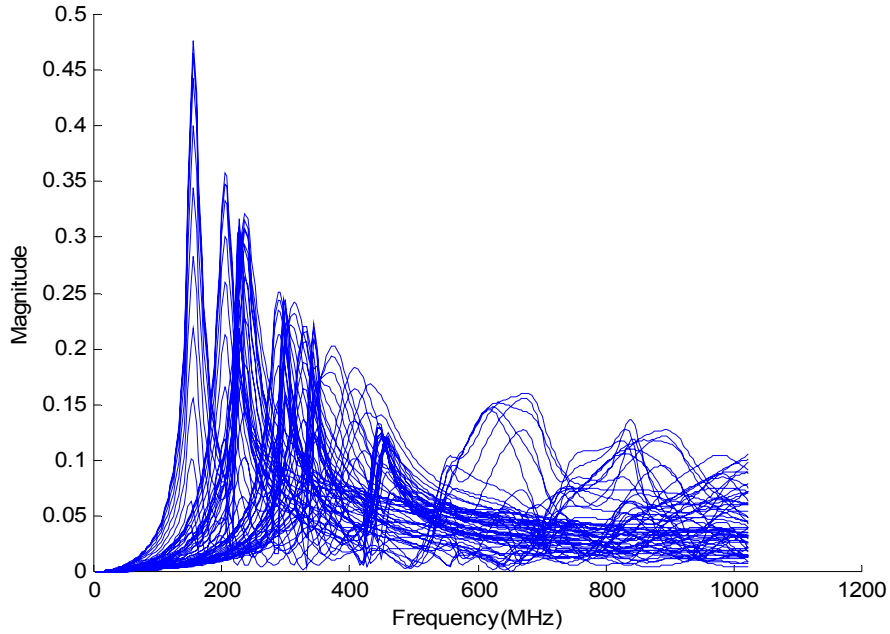

Figure 4.2 Magnitudes of unwindowed back-scattered frequency responses of all targets at all aspects (5x12=60 responses are plotted)

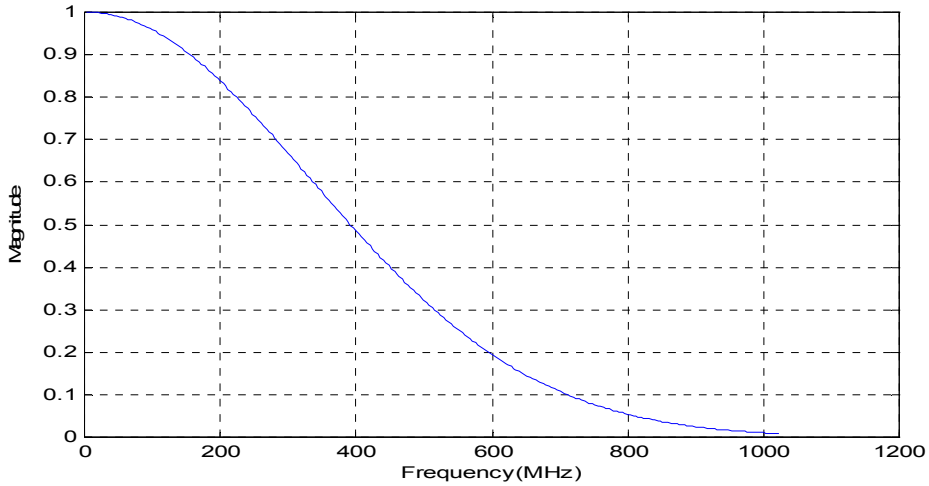

Figure 4.3 A gaussian window used to avoid Gibbs's phenomena in time-domain

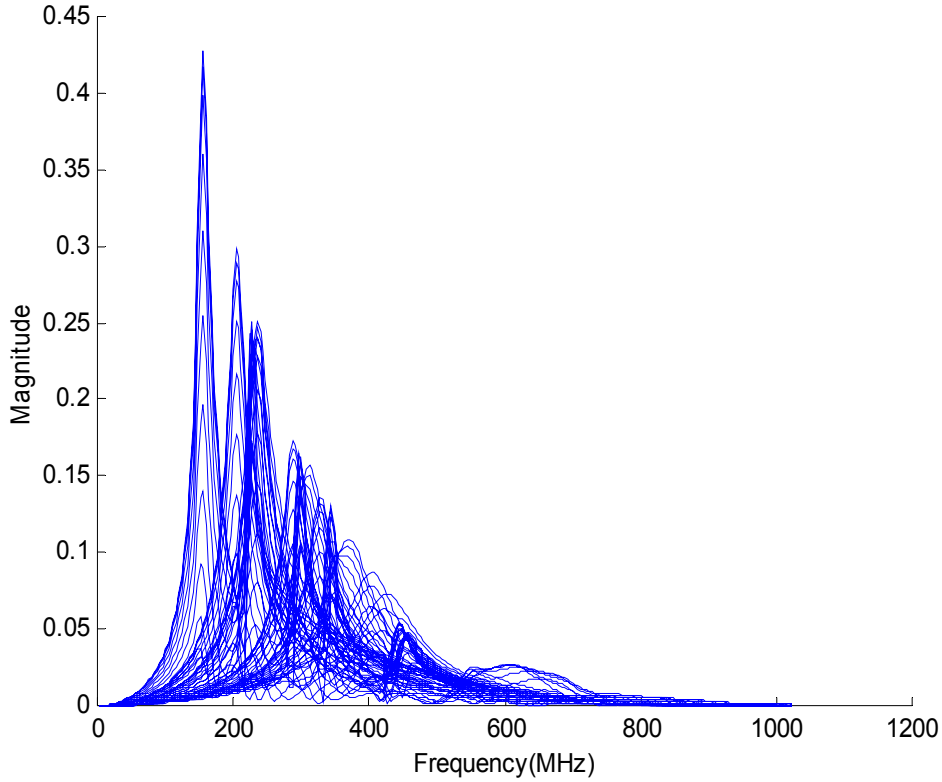

Figure 4.4 Magnitudes of windowed back-scattered frequency responses of all targets at all aspects (12x5=60 responses are plotted)

As reported earlier in this thesis, all time domain signals are normalized such that the total energy of each signal equals to unity for a fair comparison before any analysis is made on them. In general, this action is made to avoid the magnitude differences of scattered responses due to the distance between the observation point and the target and possible fluctuations of source power at the transmitter site. The normalized time domain signals obtained by taking IFFT of windowed back-scattered frequency responses shown in Figure 4.4 are plotted in Fig 4.5. Since, we use the frequency step of 4MHz with 256 frequency sample, our total time span is 250 nsec with 512 time sample. It is clearly seen that, our time span is sufficient because, all time domain signals stop oscillations and reach to zero before time span finishes.

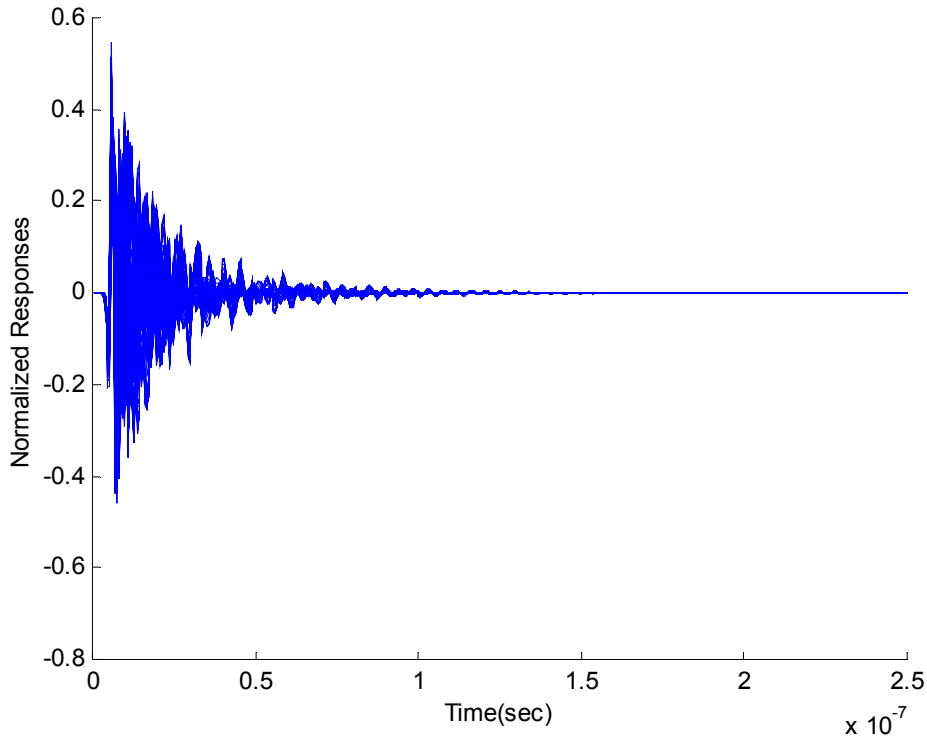

Figure 4.5 Normalized back-scattered time domain responses of all targets at all aspects (5x12=60 responses are plotted).

Therefore, we have obtained all time-domain impulse responses for all targets at all aspects. To see oscillations due to natural resonance in late-time region more clear, the signal obtained for the target 2 (Boeing 747) at the aspect of φ=30, is plotted in Fig.4.6.

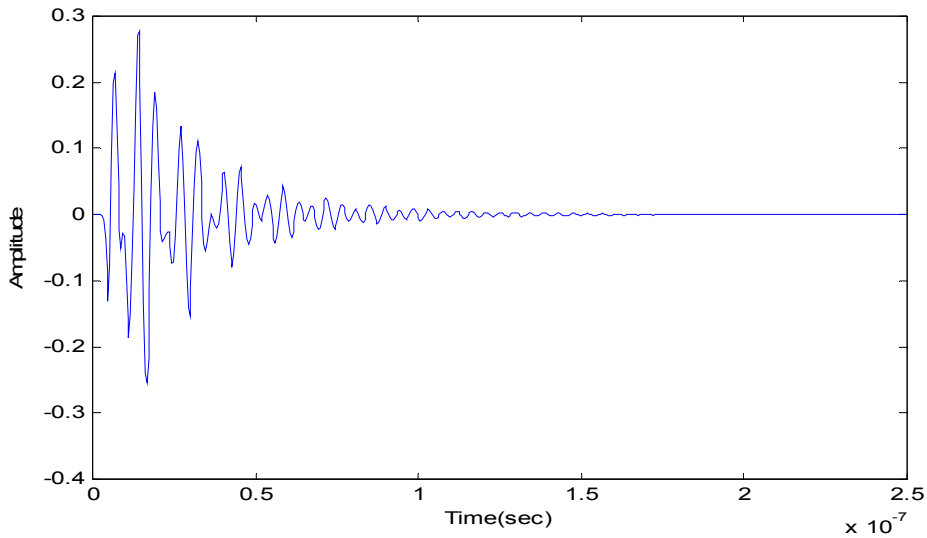

Figure 4.6 Normalized back-scattered time domain response of Target-2 (Boeing 747) at the aspect of ϑ=60 degree and φ= 30 degree

Since, Figure 4.4 does not give any detailed information about the back-scattered frequency responses of each target individually, the windowed responses of each target for some selected aspects of φ=15, 45, 75 degrees, are given in Fig 4.7, 4.8, 4.9, 4.10 and 4.11.

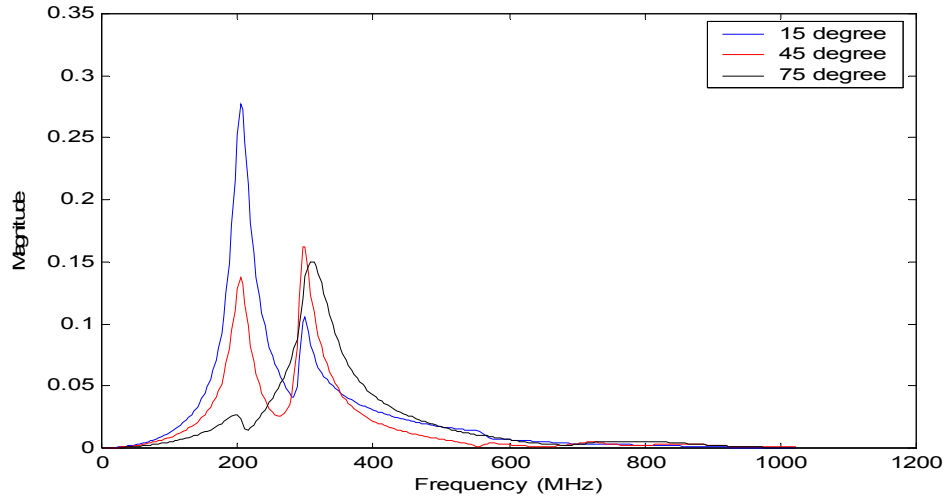

Figure 4.7 Magnitudes of windowed back-scattered frequency responses of Target 1 at the aspects φ=15, 45, 75 degrees

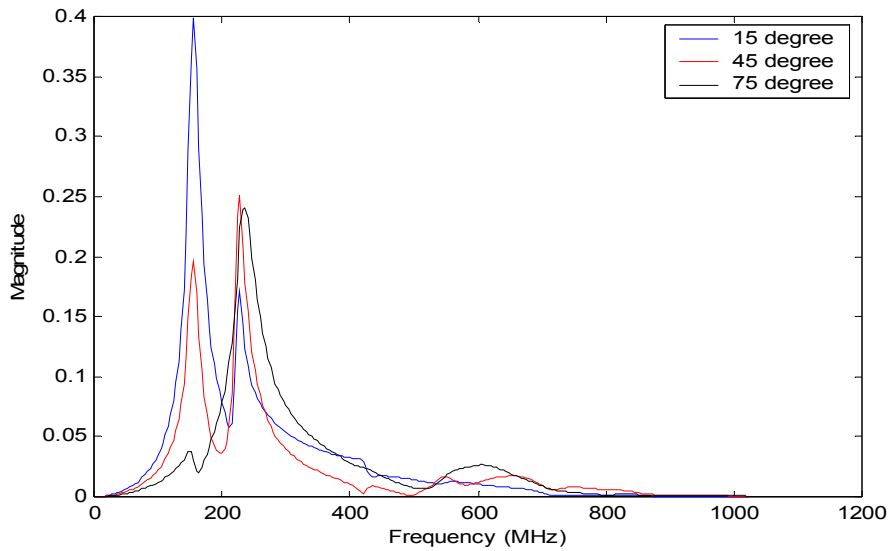

Figure 4.8 Magnitudes of windowed back-scattered frequency responses of Target 2 at the aspects of φ=15, 45, 75 degrees

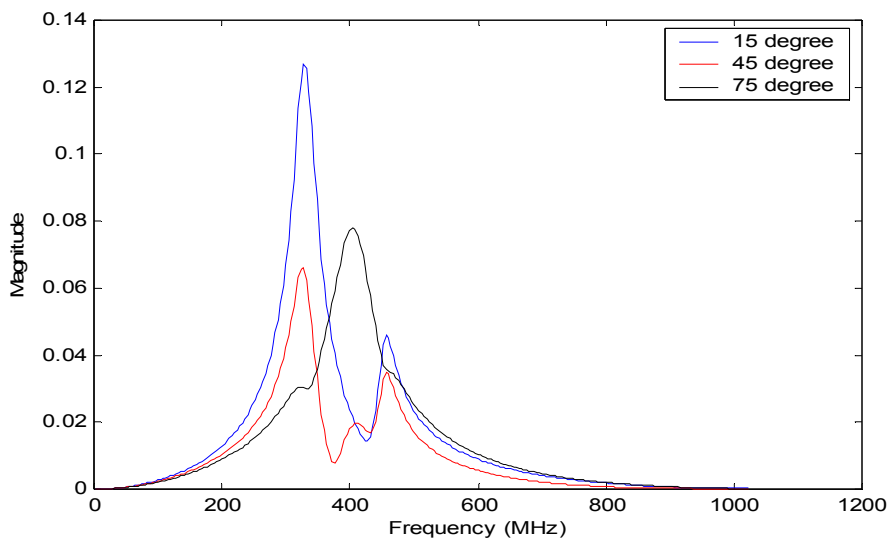

Figure 4.9 Magnitudes of windowed back-scattered frequency responses of Target 3 at the aspects of φ=15, 45, 75 degrees

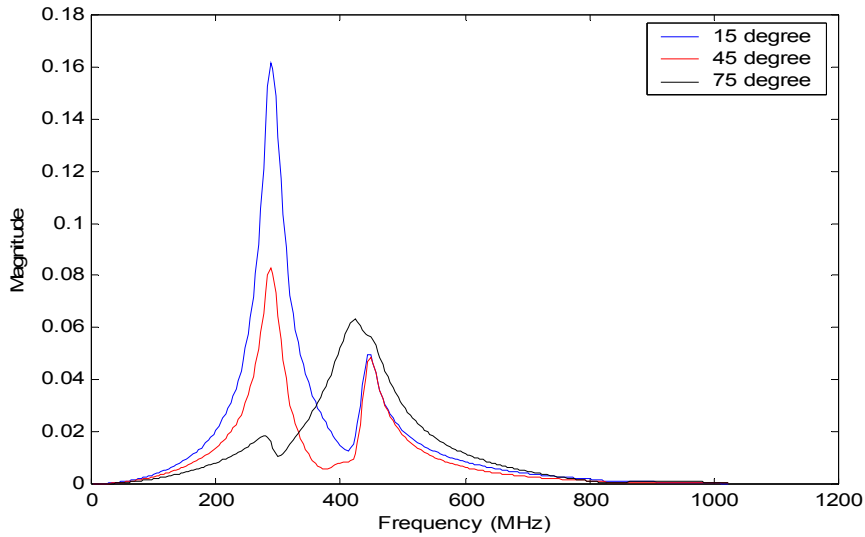

Figure 4.10 Magnitudes of windowed back-scattered frequency responses of Target 4 at the aspects of φ=15, 45, 75 degrees

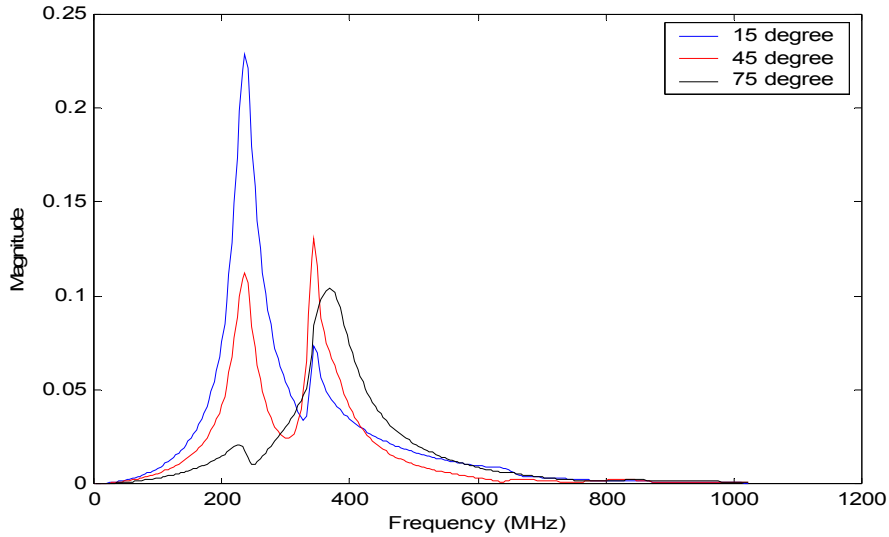

Figure 4.11 Magnitudes of windowed back-scattered frequency responses of Target 5 at the aspects of φ=15, 45, 75 degrees

As seen from the last five figures, the targets whose size larger than the others, has their first natural resonances at smaller frequencies than that of the other targets. Target 2 whose frequency response is shown in Figure 4.8, has the longest wire lengths and consequently has the smallest natural frequencies than the other targets as expected. Also for a given target, as the aspect changes, the magnitude of the natural frequencies of the associated target changes also. This is because of the aspect dependency of the residues at that natural frequency as mentioned earlier. This change can be seen more clearly at the aspect of $\varphi = 75$ degrees for each target. At this aspect, the first natural frequency of each target is excited weaker than the other aspects.

4.2. Design of the classifier database

For this target classification example, the reference aspects are chosen as φ=15, 45, 75 degree while keeping ϑ=60 degree fixed. We will determine the optimum values of Q and q* by following the method briefly explained in Sections 2.4 and 2.5. We have 5 targets and 3 reference aspects, so the total number of signals in the reference database is 15. We start with the process of determination of the optimum value of Q.

The procedure explained in Section 2.5 for a Q set of (8, 16 and 32) will be illustrated here. For each target, partitioned energy density vectors defined on full time span 250 nsec ($\overline{E}$'s as given by Equation (2.11)), are constructed for each of the back-scattered data for all 3 reference aspects. Then, one of $\overline{E}$ vectors for example the one that is associated with φ=15 degree reference aspect, is chosen among them to compute the correlation coefficients between this $\overline{E}$ vector and the other two $\overline{E}$ vectors associated with the other reference aspects. Hence, each target's the correlation coefficients graphs between partitioned energy density vectors of reference aspects, was obtained. All the process is repeated for all values of Q in the set. The aim here is to determine a proper Q value which leads to minimal variation in correlation coefficients within each individual target reference database for the purpose of reducing aspect sensitivity of extracted feature vectors.

The results are shown in Fig 4.12, 4.13 and 4.14 for Q values of 8, 16 and 32, respectively. Index of reference aspects in the figures denotes φ=15, 45 and 75 degrees as 1, 2 and 3, respectively. It is seen that for all values of Q, correlation coefficient between partitioned energy density vectors of reference aspect φ=45 and φ=15 is high as much as 0.8 for all targets, but correlation coefficient between partitioned energy density vectors of reference aspect φ=75 and φ=15 is low down to 0.2 denoting high aspect dependency.

.

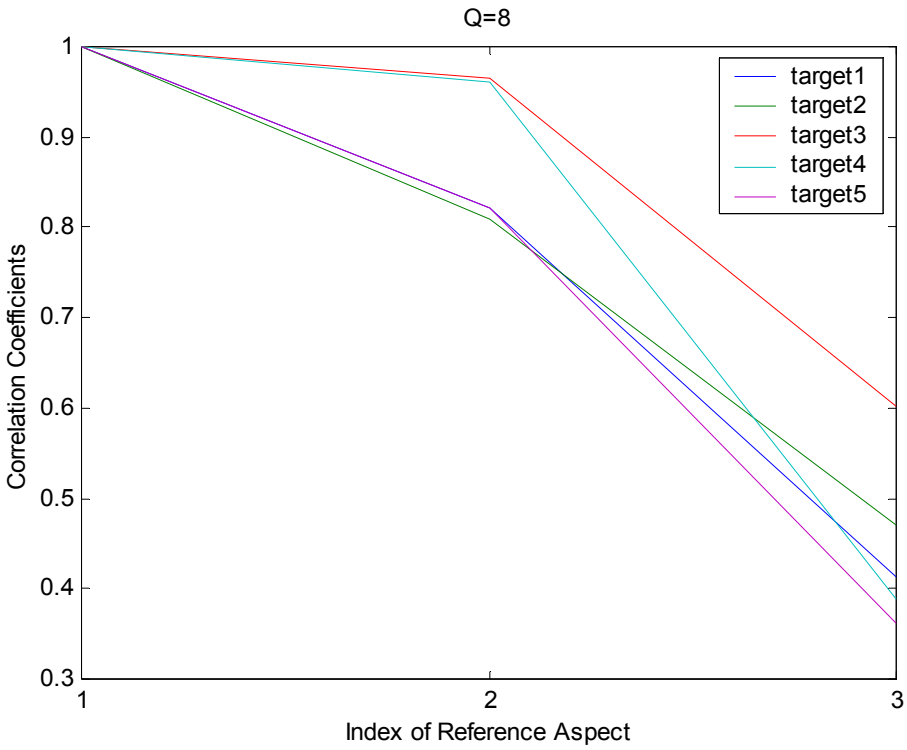

Figure 4.12 Correlation Coefficients between the partitioned energy density vectors of reference aspects and that of φ=15 degree reference aspect for each target for Q=8.

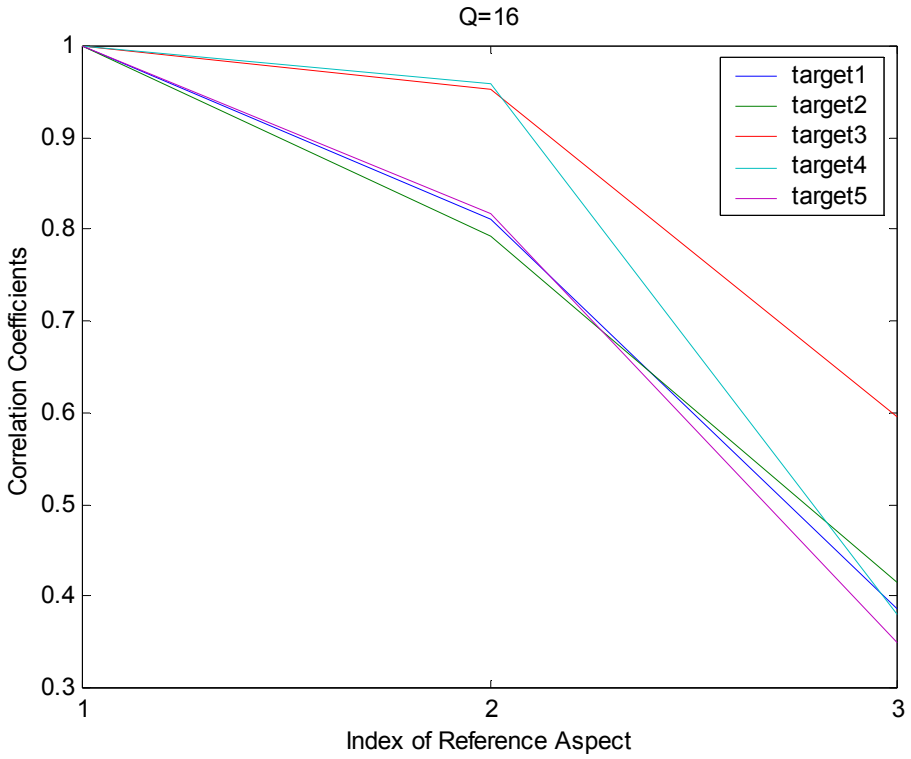

Figure 4.13 Correlation Coefficients between the partitioned energy density vectors of reference aspects and that of φ=15 degree reference aspect for each target for Q=16.

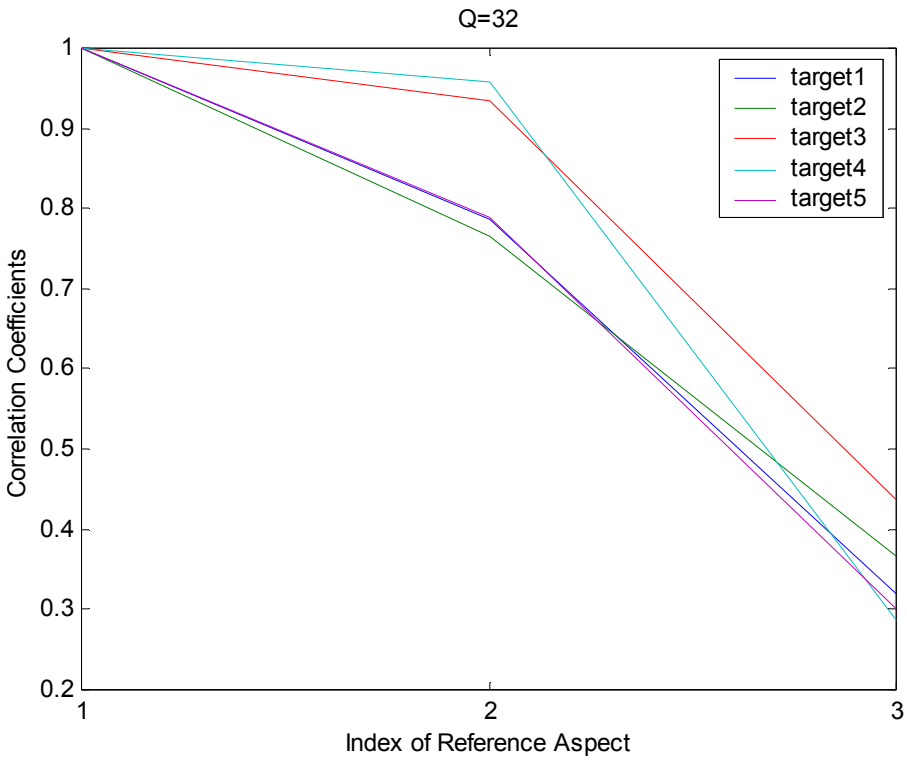

Figure 4.14 Correlation Coefficients between the partitioned energy density vectors of reference aspects and that of φ=15 degree reference aspect for each target for Q=32.

It is not easy to see which value of Q has the smallest variance for each target by examining Figures 4.12, 4.13 and 4.14. Hence, the variances of each correlation coefficients plot for each target, and for each value Q is given in Figure 4.15 corresponding to step 4 in Section 2.5.

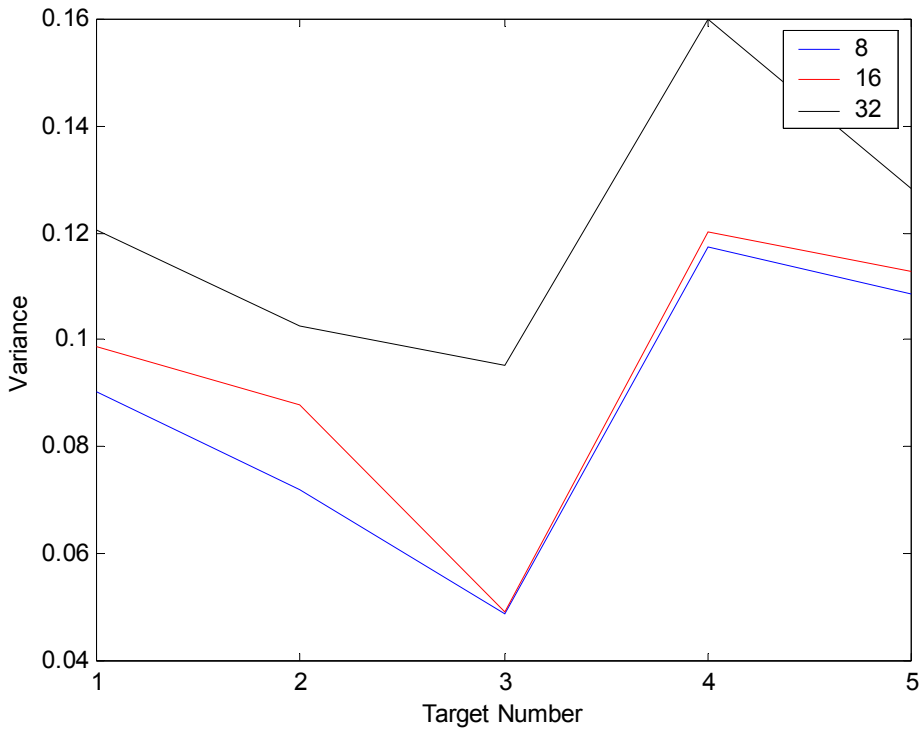

Figure 4.15 Variance graph for Q=8, 16 and 32 for each target

The optimum value of Q must correspond to the smallest value of the computed variances as indicated in Section2.5. From Figure 4.15, we see that, Q=8 value has the smallest variances for all targets, but Q=16 plot is also very close to the plot of Q=8. Since Q value determines how many subintervals that total time span T_0 would be divided into, as Q gets smaller, each subinterval becomes wider. Later, when we will select q*, two successive time bands in Q=8 case has sample size of 512 x (2/8) =128 in the total of 512. Integration over such a large time span while constructing LTFVs might impair temporal accuracy. For that reason, we select Q=16.

After selecting optimum value of Q, we will determine q* by calculation CCF (Equation (2.13)) of each q* from 1 to Q-1. Since we have 5 target and 3 reference aspect K=5 and M=3, then Equation (2.13) becomes

$$CCF\ (q^*) = \frac{1}{5\,x\,9}\sum_{i,j} r_{i,j}^{matched} - \frac{1}{20\ *\ 9}\sum_{i,j} r_{i,j}^{mismatched} \qquad (4.1)$$

Since there is 5 matched and 20 mismatched block on the on the correlation coefficients table each has a size MxM=9. In Figure 4.16, CCF results for each value of q* is given while keeping Q=16 fixed.

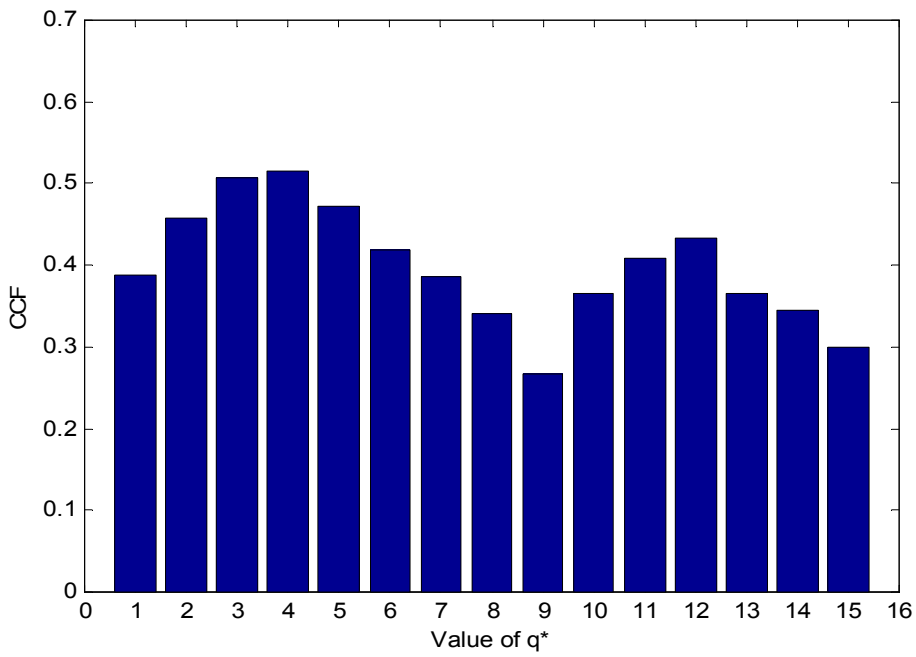

Figure 4.16 CCF as a function of q* based on the reference database

The maximum CCF corresponds to q*=4; which determines LTFV $\overline{e}$. That means Equation (2.12) becomes

$$\overline{e} = [\overline{E}_4 \quad \overline{E}_5 \ ] \tag{4.2}$$

By examining Fig 4.16, the second highest q*=3 that corresponds to a LTFV of $\overline{e} = [\overline{E}_3 \quad \overline{E}_4 \ ]$. This gives idea of using only $\overline{E}_4$ as LTFV. The performance results of the classifier will support the idea in Section 4.3.

A question may arise because of the solution of q* that gives maximum CCF value is 4. Are we in the late-time region that contains natural resonance related components? This question will be answered by looking time-responses of reference aspects on which q* determination was done. The time region on which we work is, corresponding to $\overline{E}_4$ for all signals, between 46.875nsec and 62.5nsec. Taking the normalized signals obtained from target 2 (Boeing 747) at reference aspects of φ=15, 45, 75 as in Figure.4.17 a, b, c respectively and looking the specified time interval [46.875-62.5] nsec corresponding to [96-128] time samples range. It is seen from the figure that, φ=15 and 45 degrees responses are oscillating up to 300th -350th time samples (Figure 4.17a and 4.17b), but φ= 75 degrees response (Figure 4.17c) approximately vanishes after 160th time sample. Since, the location of late-time regions are highly aspect dependent and we must catch natural resonance related components in late-time region for all aspects, we must take into account the reference signal which vanishes at the earliest time like in the case of φ= 75 degrees. But also we must avoid the early-time region of any aspect's responses. Taking a look at φ= 15 degrees and [96-128] time samples region again, we see that, we are not in early-time region, so the selection of $\overline{E}_4$ as LTFV was not physically wrong.

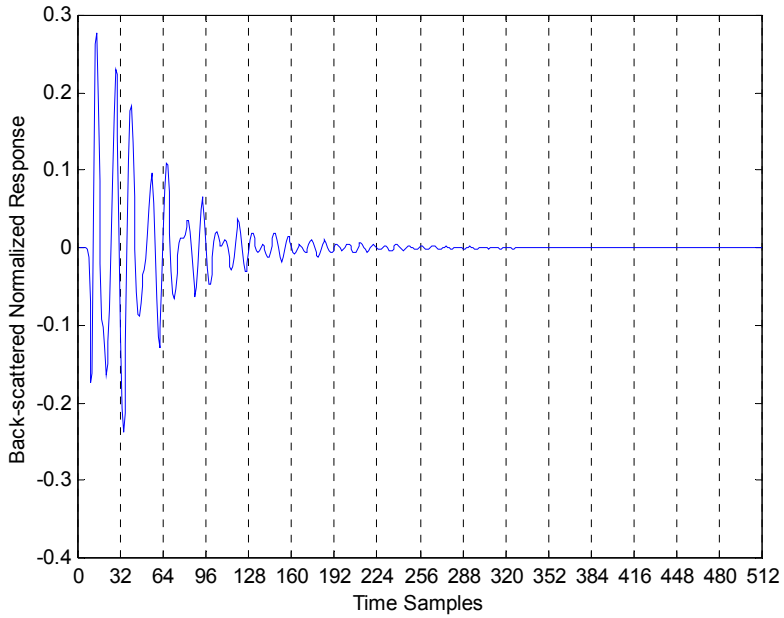

Figure 4.17a Normalized back-scattered time domain responses of Target-2 (Boeing 747) at reference aspects of ϑ (theta) =60 degree fixed and φ (phi) = 15 degree

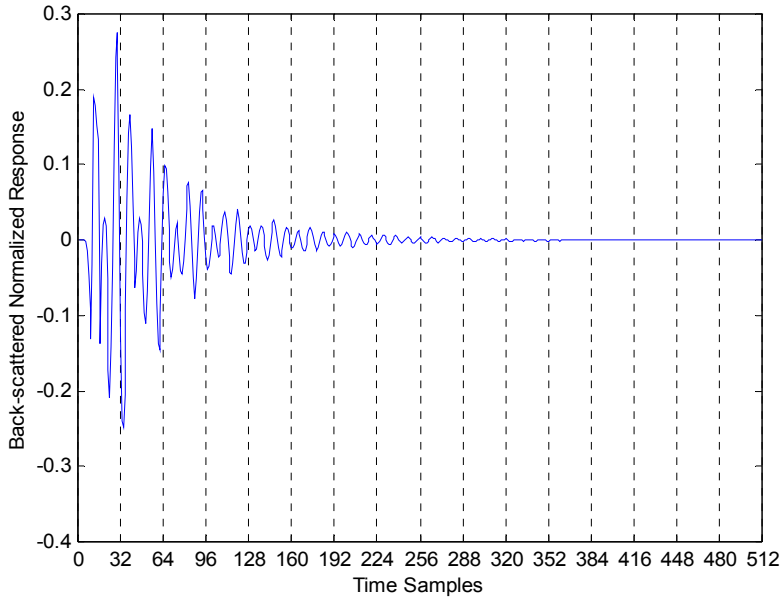

Figure 4.17b Normalized back-scattered time domain responses of Target-2 (Boeing 747) at reference aspects of ϑ (theta) =60 degree fixed and φ (phi) = 45 degree

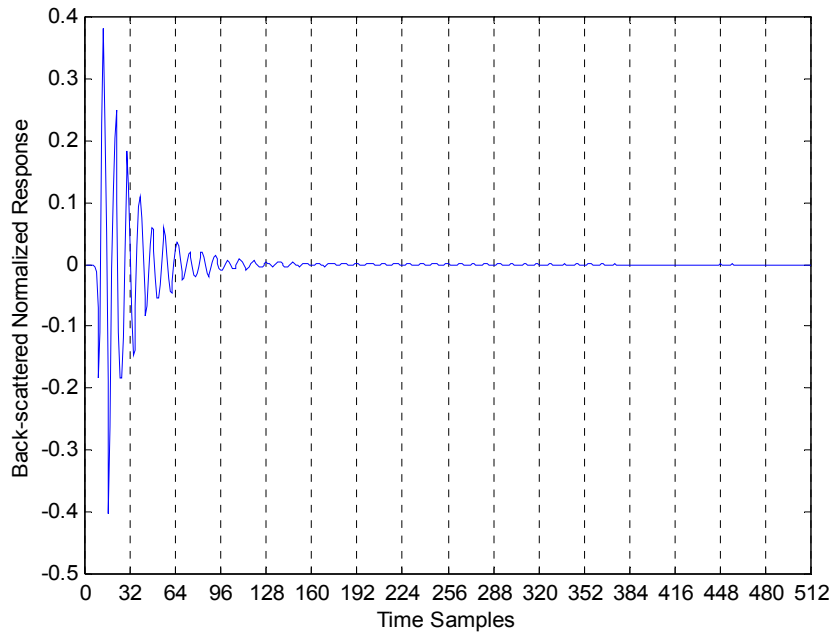

Figure 4.17c Normalized back-scattered time domain responses of Target-2 (Boeing 747) at reference aspects of ϑ (theta) =60 degree fixed and φ (phi) = 75 degree

Since, we have completed the design steps, we have used these determined values of Q and q* to construct LTFVs as explained in Section 2.4. Then by applying PCA on LTFV as explained in Section 2.6, we have constructed FFVs of each target. These intermediate steps have been done by MATLAB programs given in Appendix B. Since, all the required explanations was given in Chapter 2, they are not repeated here.

Before starting to check the performance of the classifier, we must test the validity of an assumption which we have stated in Section 2.6. We have said that using only first principal component z_1 in Equation (2.21) as a single characteristic vector (FFV) for the target of concern is enough. Now, we will check the accuracy of this assumption.

To demonstrate, we will use a different usage of CCF calculation Equation (2.13) again. Since we have 5 targets and a total of 12 aspects (i.e. K=5 and M=12), then Equation (2.13) becomes

$$CCF = \frac{1}{5\,x12}\sum_{i,j} r_{i,j}^{matched} - \frac{1}{20\ *12}\sum_{i,j} r_{i,j}^{mismatched} \qquad (4.3)$$

this time to compute CCF values using correlation coefficients between LTFVs of all aspects (M=12) and FFV of each target. In FFV computations, we used two alternatives,

$$FFV = \sum_{i=1}^{3} \overline{\lambda}_i z_i \quad \text{and} \quad FFV = z_i \quad \text{where i=1,2,3} \qquad (4.4)$$

Below is the table of CCF values computed from Equation (4.3) for four possible cases of FFV

Table 4.2 CCF values for 4 different computations of FFVs

$FFV =$	$\sum_{i=1}^{3} \overline{\lambda}_i z_i$	Only z_1	Only z_2	Only z_3
CCF	0.5114	0.5118	-0.002	0.0331

It is easily seen from Table 4.2 that choosing only the first principal component z_1 as the FFV of the target, gives the highest CCF value which is even higher than the CCF value obtained by using all three principal components. Hence, we have proven that our statement in Section.2.5 is true for our application.

The eigenvalues (λ_i's) and the percentage eigenvalues $100\overline{\lambda}_i$'s for all targets are given in Table 4.3. It is seen that for each target the eigenvalue of the first

principal component z_1, has the highest percentage value around 90%. This information proofs that using only z_1 is enough for this target set.

Table 4.3 Eigenvalues λ_i's and percentage eigenvalues 100 $\overline{\lambda_i}$'s of principal components for each target

Eigenvalues λ_i's and percentage eigenvalues 100 $\overline{\lambda_i}$'s for each target					
Ordered Eigenvalues	Target 1 (10^{-4})	Target 2 (10^{-4})	Target 3 (10^{-7})	Target 4 (10^{-7})	Target 5 (10^{-5})
λ_1	0.1279 (95%)	0.6863 (92.3%)	0.1612 (93.2%)	0.3552 (88.2%)	0.4962 (96.3%)
λ_2	0.0061 (4.5%)	0.0542 (7.3%)	0.0059 (3.4%)	0.0330 (8.2%)	0.0159 (3.1%)
λ_3	0.0006 (0.5%)	0.0029 (0.4%)	0.0058 (3.4%)	0.0147 (3.6%)	0.0033 (0.6%)

It is also important to know how much each principal component is correlated with LTFVs at reference aspects. To demonstrate, for target 2, correlation coefficients between LTFVs at reference aspects and each principal component, are given in Table 4.4. It is seen that z_1 has the highest correlation coefficients with LTFV of each reference aspect except LTFV at φ=75. Using z_3 while constructing FFV of this target is useless because its contribution to FFV of target 2 is only 0.4%. Also z_3 gives very low correlation coefficients with LTFVs at other reference aspect.

Table 4.4 Correlation coefficients between LTFVs at reference aspects and each principal component for Target 2

Principal Components	LTFV at φ=15	LTFV at φ=45	LTFV at φ=75
z_1	0.8846	0.9894	0.6559
z_2	-0.4662	0.1452	0.3513
z_3	0.0094	-0.0081	0.6681

LTFVs at each reference aspect and the FFV using only first principal component z_1 for each target, are plotted in Figures 4.18, 4.19, 4.20, 4.21 and 4.22 respectively.

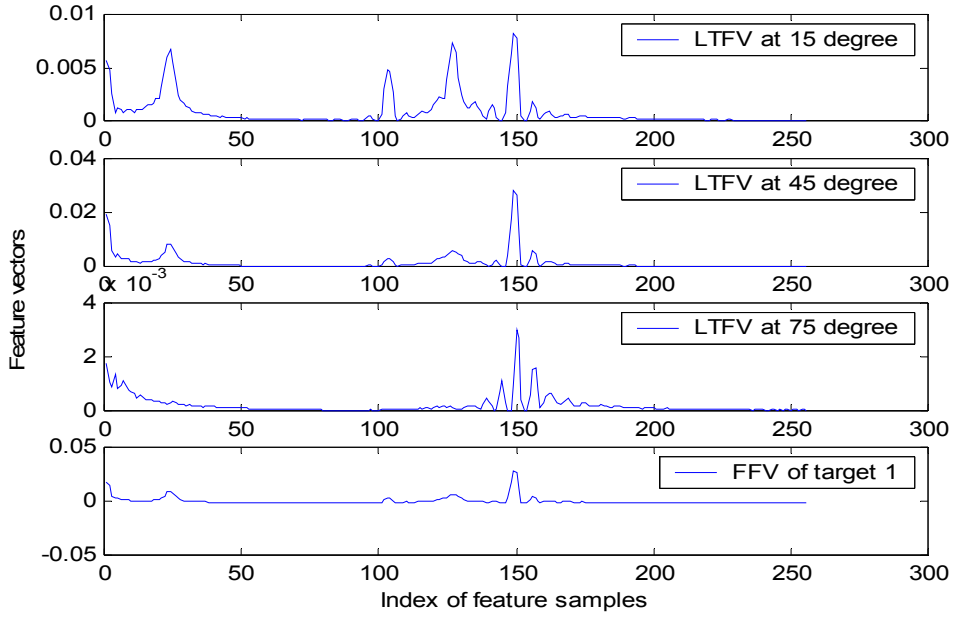

Figure 4.18 LTFVs for each reference aspect and FFV of Target 1

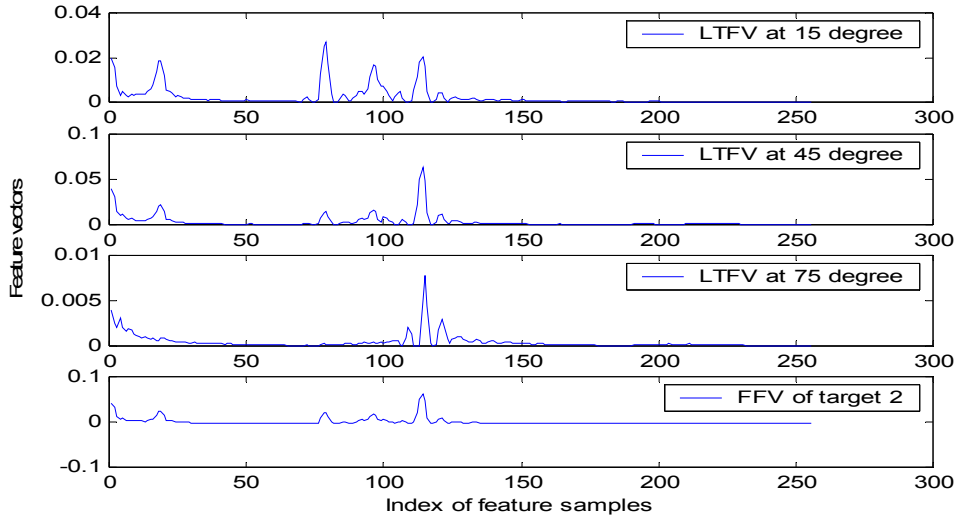

Figure 4.19 LTFVs for each reference aspect and FFV of Target 2

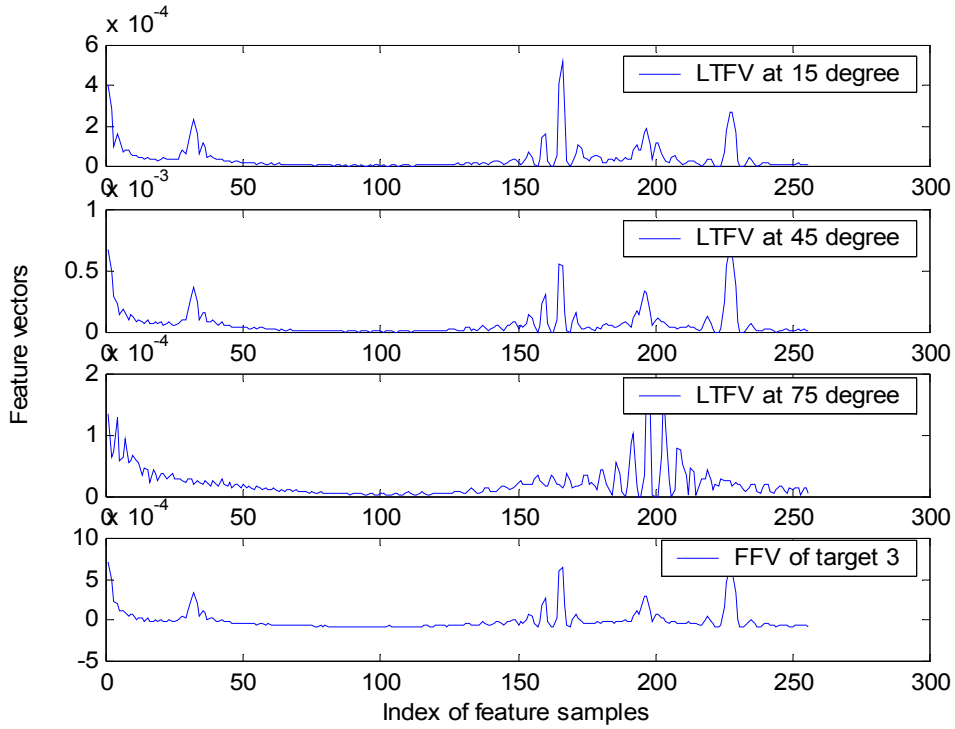

Figure 4.20 LTFVs for each reference aspect and FFV of Target 3

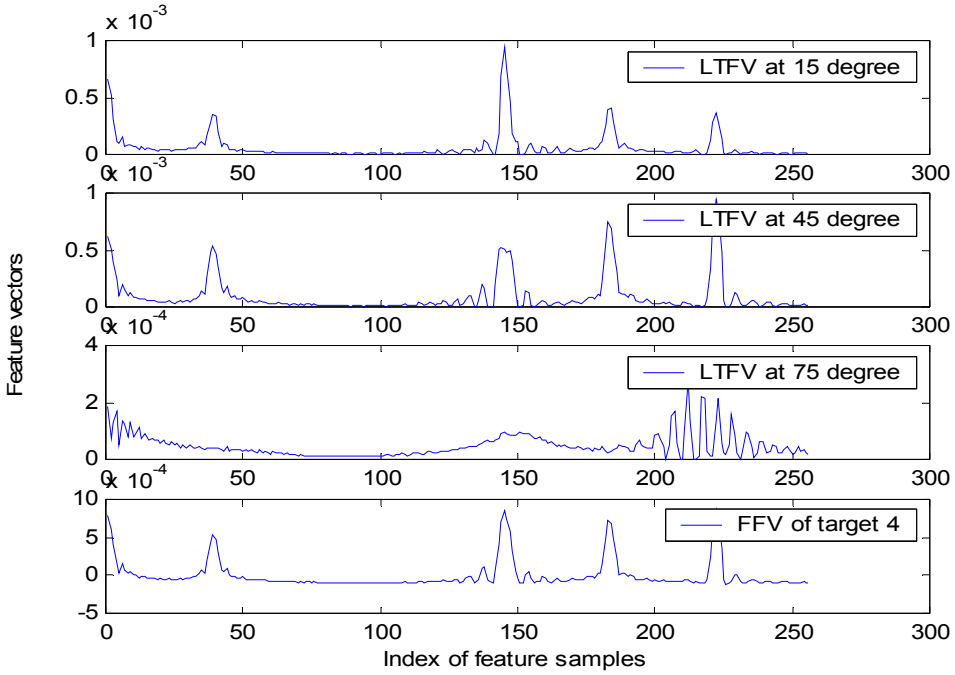

Figure 4.21 LTFVs for each reference aspect and FFV of Target 4

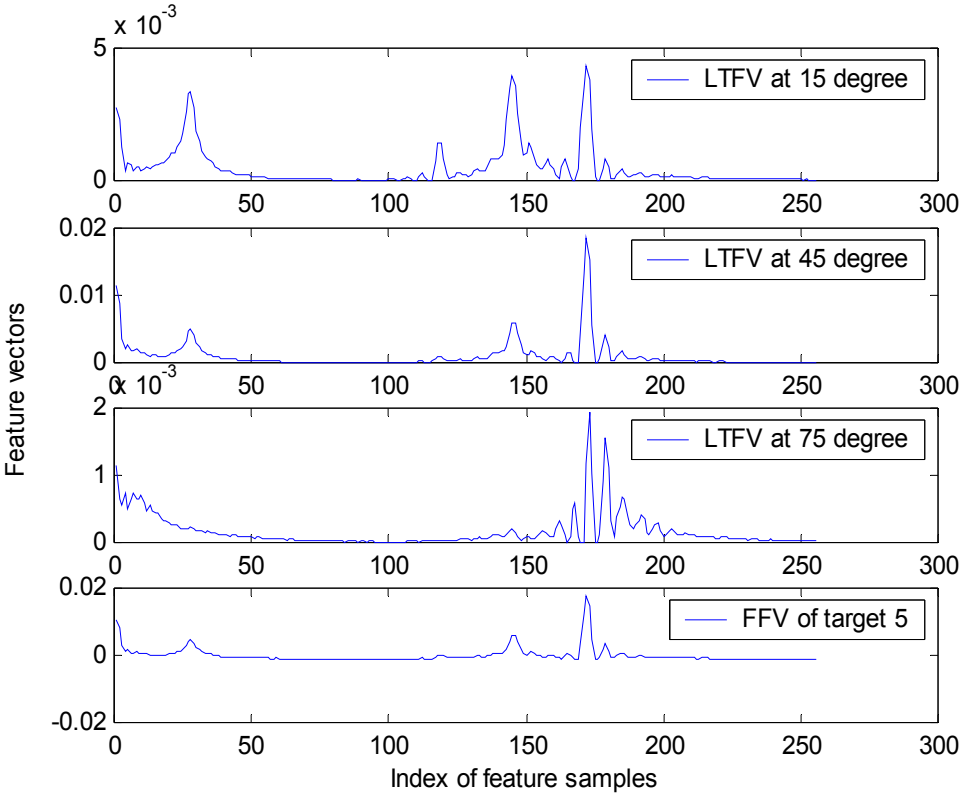

Figure 4.22 LTFVs for each reference aspect and FFV of Target 5

4.3. Performance test of the classifier

After obtaining FFV of each target, we have only 5 vectors corresponding to 5 targets, each has length of N/2, where N is length of the scattered signals. Hence, we gain from dimensionality consequently from decision time. The performance test of the classifier will be done by comparing LTFVs of signals from 9 test aspects for each target with these 5 FFVs. Then, decision can be made by using three different criteria which are defined in [2] as;

1. Maximum reference match (MRM) criterion looks for the reference index that corresponds to the highest correlation coefficient between the tested signal/feature and the reference signals/ features. The classifier's decision is made in favor of the target class associated with this index.

2. Complete class match (CCM) criterion looks for a matching target class whose reference signals/features have the highest correlation coefficients with respect to the tested signal/feature at all reference aspects (i.e., all the other target classes at all reference aspects produce lower correlation coefficients).

3. Complete class match with at least 5 percent contrast margin (CCM-5%) criterion looks for the CCM criterion with an additional requirement that the maximum of the mismatched correlation coefficients is at least 5 percent lower than the minimum of the matched correlation coefficients to reduce decision uncertainty. If desired, this safety margin can be increased to test the robustness of the classifier for highly noisy data in particular.

Actually, MRM and CCM is the same for a FFV based classifier. The correct decision rate is then computed as the percentage of the number of correct decisions in total number of decisions.

To test our classifier correlation coefficients graph is computed between LTFVs of each test signal and 5 FFVs as shown in Fig 4.23. Since, we have 9 test aspect φ (phi) =5, 10, 22.5, 30, 37.5, 52.5, 60, 67.5, 82.5 degrees for each target, there are 45 test signal. The indices in the Figure 4.23, are arranged such that the indices 1 to 3 corresponds to FFV of target 1, indices 4 to 6 corresponds to FFV of target 2 and so on for horizontal axis; the indices 1 to 9 corresponds to LTFVs of target 1's test signals, the indices 10 to 18 corresponds to LTFVs of target 2's test signals and so on for vertical axis.

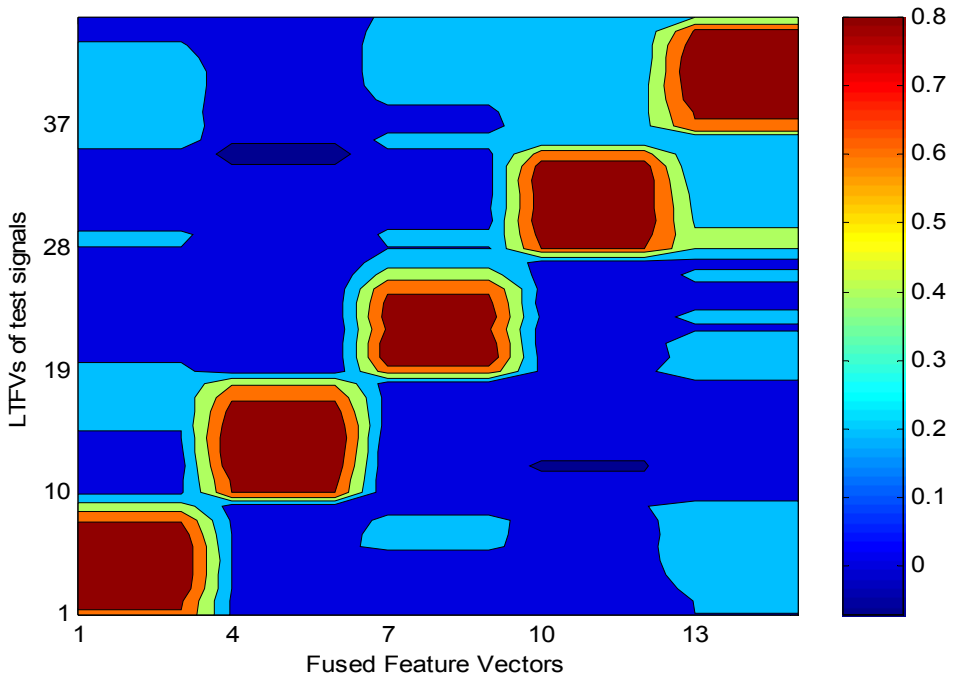

Figure 4.23 Correlation coefficients graph is computed between LTFVs of test signal and 5 FFVs of targets.

Correct decision rate is computed in MATLAB, and the result is 97.8% denoting only 1 error for 45 test signals based on CCM criterion, and 95.6% for CCM5 criterion denoting 2 errors for 45 test signals and more importantly remains same 95.6% for CCM25 criterion with 25% safety margin. These values states that our classifier has reached high decision rates.

While determining the design parameters of the classifier in Section 4.2, we have selected Q as 16 instead of 8. The effect of this choice to the performance of the classifier is tested here by selecting Q as 8. In Figure 4.24, CCF result for each value of q* are given

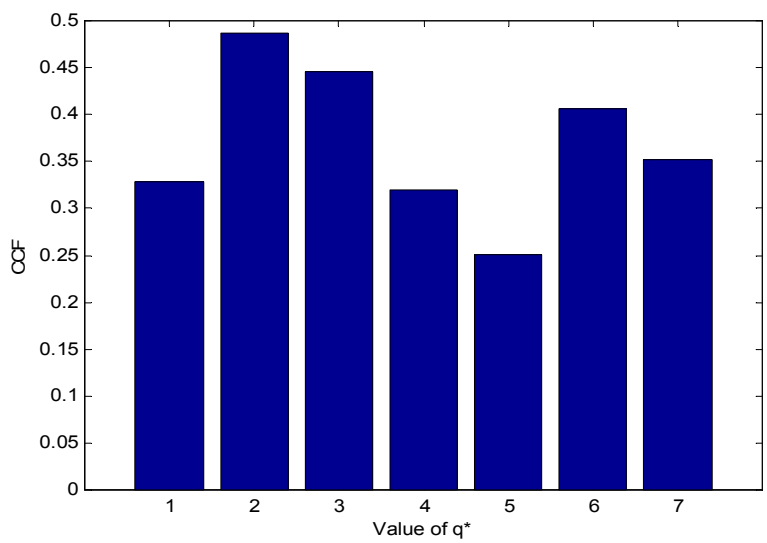

Figure 4.24 CCF as a function of q* based on the reference database

We select q* as 2 since it gives the maximum correct classification factor and obtain the LTFVs accordingly as $\overline{e} = [\overline{E}_2 \quad \overline{E}_3]$. After applying PCA technique as mentioned earlier, the resulting correlation coefficients graph between LTFVs of each test signal and 5 FFVs is shown in Fig 4.25. The arrangement of indices is same as Fig 4.23.

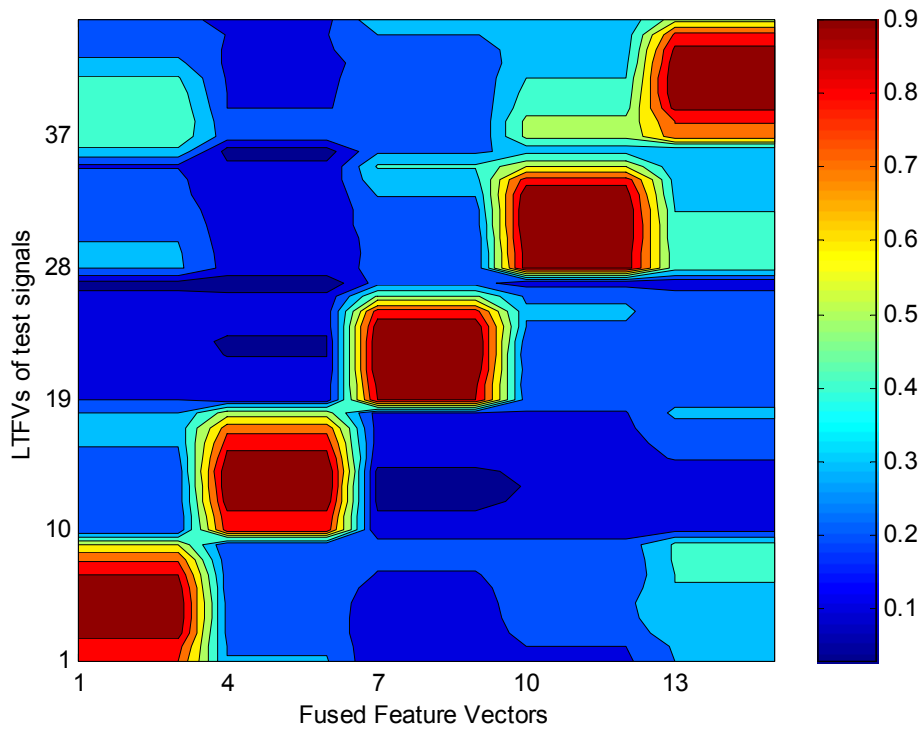

Figure 4.25 Correlation coefficients graph is computed between LTFVs of test signal and 5 FFVs of targets (Q=8 and q*=2)

Correct decision rate is computed in MATLAB, and the result is 95.6% denoting 2 errors for 45 test signals based on CCM criterion, while the result of our original design parameters 97.8% denoting only 1 error for 45 test signals based on CCM criterion. CCM5 and CCM25 results are same with the original results. Therefore, a little but important improvement in the performance of the classifier based on CCM criterion, have been obtained by selecting Q as 16, although Q=8 case has had the smallest variances for all targets as shown in Fig.4.15.

The other design parameter, q* have been determined as 4 from Fig 4.16 as the maximum CCF corresponds to q*=4. That means LTFV $\bar{e}$ = [$\bar{E}_4$ $\bar{E}_5$], but we have selected using only $\bar{E}_4$ as LTFV for the reason mentioned before. We now test $\bar{e}$ = [$\bar{E}_4$ $\bar{E}_5$] case while keeping Q=16 fixed. After obtaining LTFVs for the new selection and applying PCA to the LTFVs of reference aspects for each target,

the resulting correlation coefficient graph between LTFVs of each test signal and 5 FFVs as shown in Fig 4.26. The arrangement of indices is same as Fig 4.23 again.

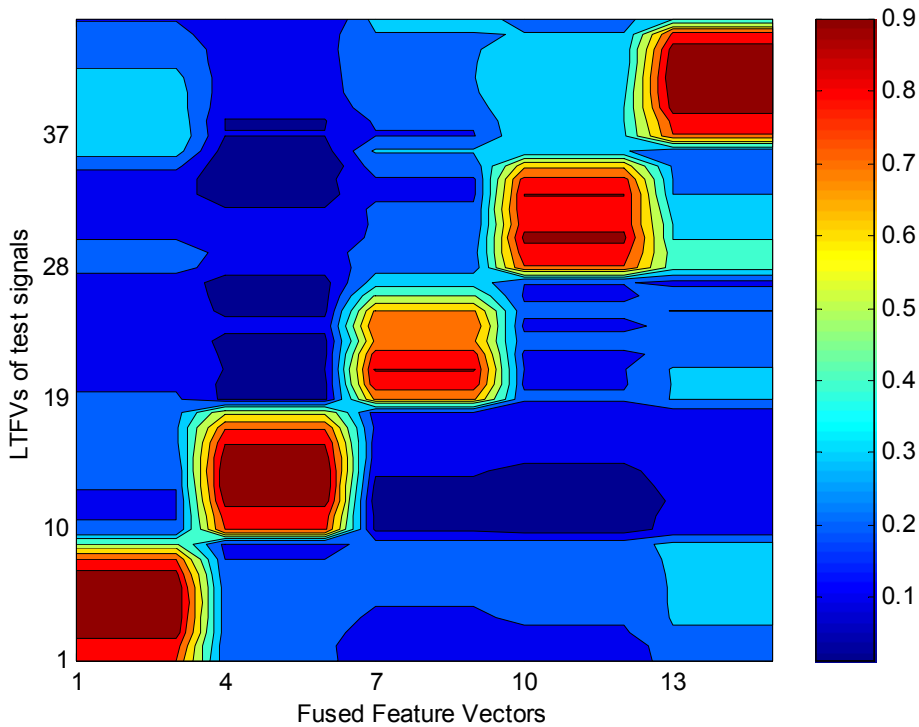

Figure 4.26 Correlation coefficients graph is computed between LTFVs of test signal and 5 FFVs of targets for LTFVs selection as $\overline{e} = [\overline{E}_4 \quad \overline{E}_5]$

Correct decision rate is computed in MATLAB, and the result is 95.6% denoting 2 errors for 45 test signals based on CCM criterion, while the result of our original design parameters 97.8% denoting only 1 error for 45 test signals based on CCM criterion. CCM5 result is same with the original results. CCM25 result give 3 error denoting 93.3% correct decision rate while the result of our original design parameters 95.6%. Therefore, an improvement in the performance of the classifier based on both CCM and CCM25 criteria have been obtained by selecting only $\overline{E}_4$ as LTFV.

Going back the original design parameters, and to demonstrate the effect of PCA on the performance of the classifier, the case in which PCA is not used is investigated. This time decision is made by comparing LTFVs of signals from 9 test aspects for each target with LTFVs of signals from 3 reference aspects for each target as shown in Fig 4.27. The indices in the Figure 4.27, are arranged such that the indices 1 to 3 corresponds to LTFVs at reference aspects of target 1 and the indices 4 to 6 corresponds to LTFVs at reference aspects of target 2 so on for the horizontal axis; the indices 1 to 9 corresponds LTFVs of target 1's test signals and the indices 10 to 18 corresponds to LTFVs of target 2's test signals so on for the vertical axis.

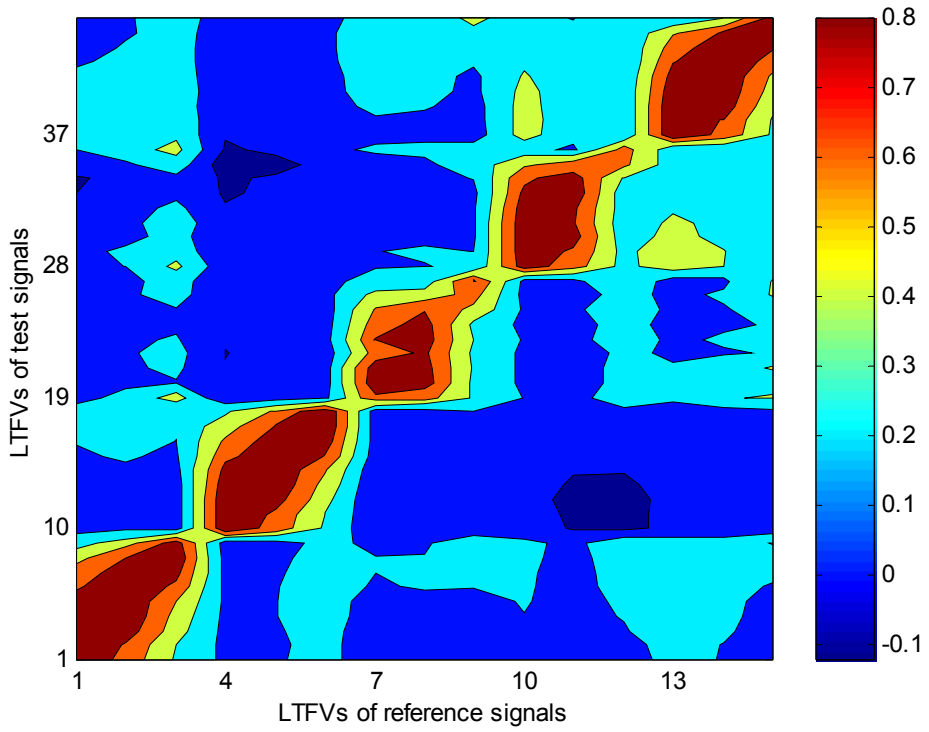

Figure 4.27 Correlation coefficients graph is computed between LTFVs of each test signal and LTFVs of each reference signal

Correct decision rate is computed in MATLAB again, and the result is 68.9 % denoting 14 errors for 45 test signals based on CCM criterion, representing a loss of performance occur. But MRM criterion gives 100 % correct decision rate.

Next, the performance of unprocessed scattered signals on full time span will be investigated. This time, decision is made by comparing scattered signals from 9 test aspects for each target with scattered signals from 3 reference aspects for each target as shown in Fig 4.28. The indices in the Figure 4.28, are arranged such that the indices 1 to 3 corresponds to scattered signals at reference aspects of target 1 and the indices 4 to 6 corresponds to scattered signals at reference aspects of target 2 so on for the horizontal axis; the indices 1 to 9 corresponds to scattered test signals of target 1 and the indices 10 to 18 corresponds to scattered test signals of target 2 so on for the vertical axis.

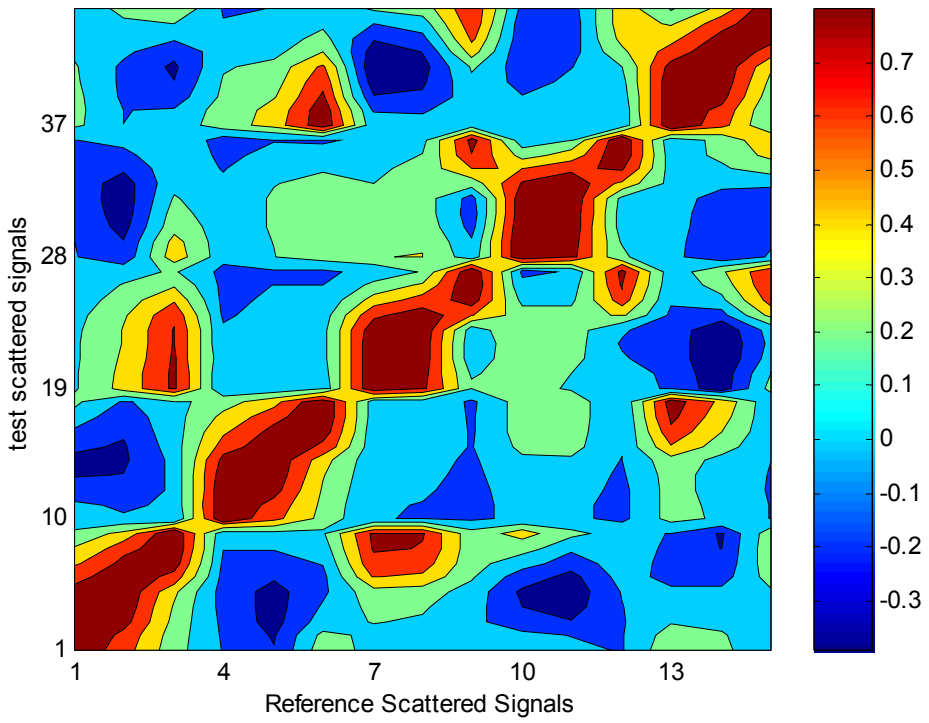

Figure 4.28 Correlation coefficients graph is computed between full time test scattered signals and full time reference scattered signals

Correct decision rate of the full time scattered signal based classifier is computed in MATLAB again, and the result is 26.7 % denoting 33 errors for 45 test signals based on CCM criterion. But applying the MRM criterion instead, gives 100% correct decision rate. The correct decision rates obtained for different criteria and classifier types are tabulated in Table 4.5 for a quick comparison.

Table 4.5 Correct Decision Rates for different criteria and classifier types

Classifier Type	MRM	CCM	CCM5	CCM25
FFV based	97.8%	97.8%	95.6%	95.6%
LTFV based	100%	68.9 %	68.9 %	53.3%
Full Time Scattered signal based	100%	26.7 %	26.7 %	15.6 %

Although CCM, CCM5 and CCM25 results show a remarkable improvement when using our natural resonance based feature extraction technique with PCA, the results for MRM criterion are all very high. Even the classifier based on full time scattered signals gives 100% correct decision rate with no feature-extraction technique. It must be remembered that MRM criterion looks for only the highest correlation coefficient match while the CCM criterion demands that all the mismatched target classes at all reference aspects must produce lower correlation coefficients than the matched target class.

After noticing that the full-time signal based classifier already shows a satisfactory classification performance (at least for the MRM criterion case), we have decided to check if the performance of the classifier can be improved by using the late-time scattered signals directly, without using the WD-based LTFV extraction. For this process, we have used the same late-time interval [46.875-62.5] nsec that has been used for LTFV extraction.

Correlation coefficients computed between the reference scattered signals and the test scattered signals over the late-time interval [46.875-62.5] nsec are plotted in Fig 4.29. The arrangement of signal indices is same as that of Fig 4.28.

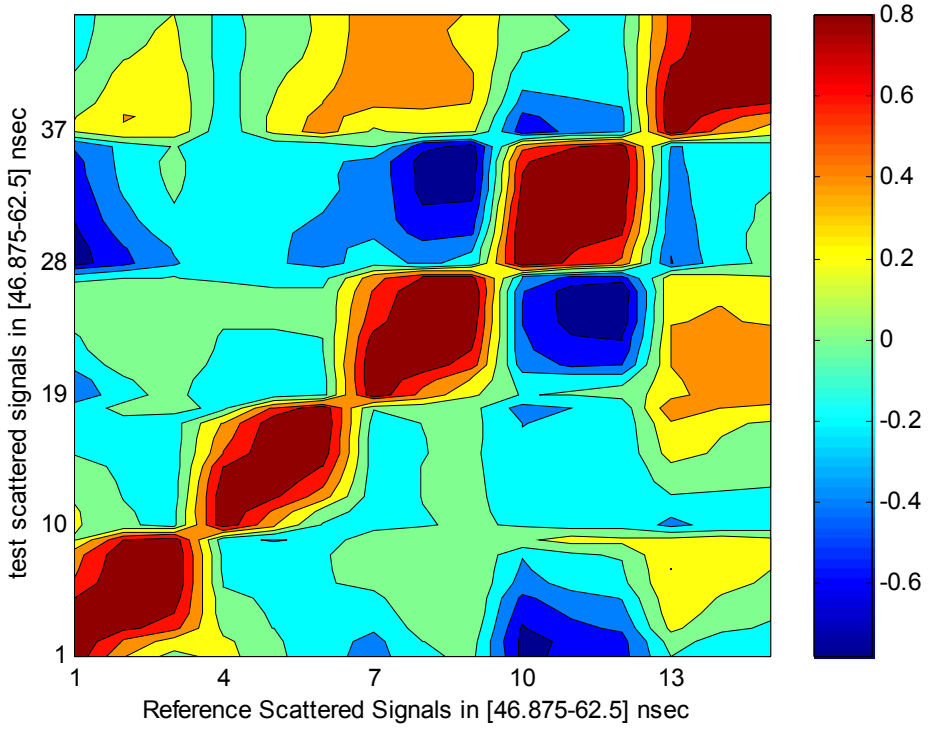

Figure 4.29 Correlation coefficients graph is computed between test scattered signals and reference scattered signals (all scattered signals in [46.875-62.5] nsec time interval)

Similarly, Fig 4.30 presents the correlation coefficient map which is obtained when the PCA technique is applied to the full time scattered signals at the reference aspects. Fig 4.31, on the other hand, presents the resulting correlation coefficient map when we apply the PCA technique to the late-time scattered signals at the reference aspects instead.

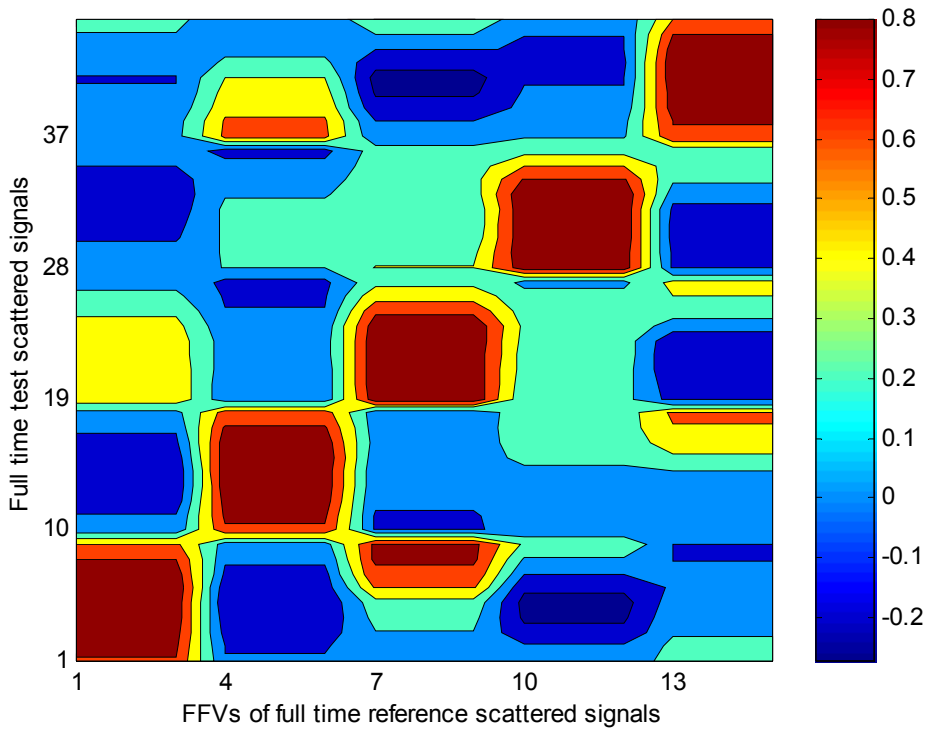

Figure 4.30 Correlation coefficients graph is computed between full time test scattered signals and FFVs of full time reference scattered signals

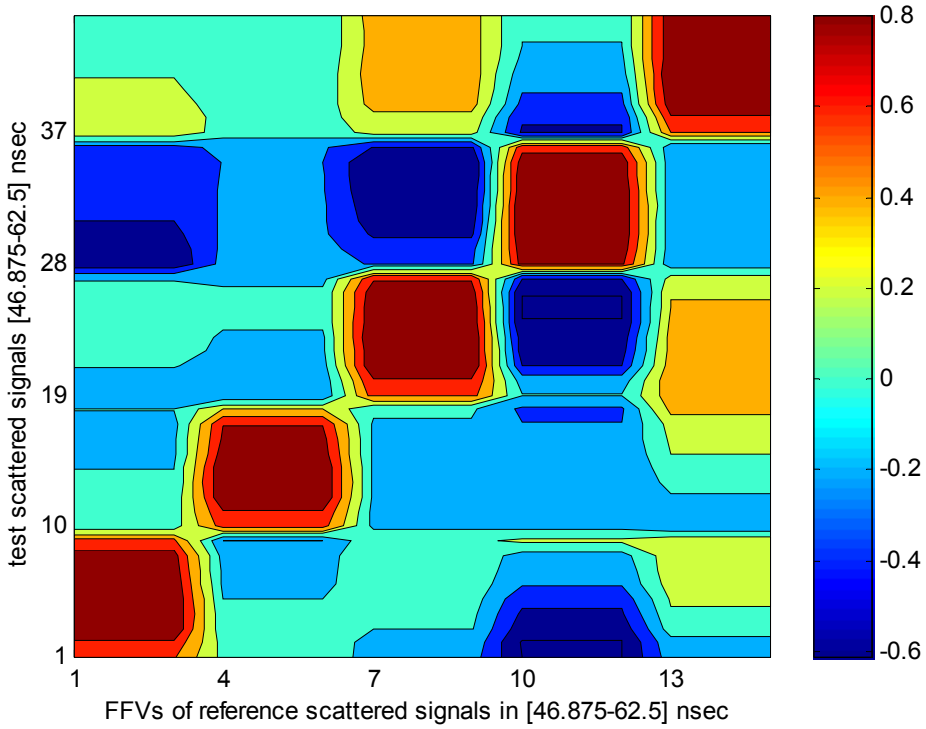

Figure 4.31 Correlation coefficients graph is computed between test scattered signals in [46.875-62.5] nsec and FFVs of reference scattered in [46.875-62.5] nsec

For a quick comparison, the correct decision rates obtained for different criteria and for various classifiers (including the newly added three classifier types) are tabulated in Table 4.6 below, which is the extended version of Table 4.5.

Table 4.6 Correct Decision Rates for different criteria and extended classifier types

Classifier Type	MRM	CCM	CCM5	CCM25
FFV based	97.8%	97.8%	95.6%	95.6%
LTFV based	100%	68.9 %	68.9 %	53.3%
Full Time Scattered signal based	100%	26.7 %	26.7 %	15.6 %
Full Time Scattered signal based + PCA	88.9%	88.9%	86.7%	71.1%
[46.875-62.5] nsec Scattered signal based	100%	82.2%	82.2%	66.7%
[46.875-62.5] nsec Scattered signal based + PCA	97.8%	97.8%	97.8%	95.6%

These new results show us that, applying PCA directly to the [46.875-62.5] nsec time interval of the scattered signals, provides the same correct classification rate (95.6% for CCM25 criterion) with the FFV based classifier that makes use of the WD-based late-time feature vectors extracted over the same [46.875-62.5] nsec time interval. The windowed frequency responses of each target at the reference aspects of

φ=15, 45, 75 degrees, were given in Figures 4.7, 4.8, 4.9, 4.10 and 4.11. The natural resonance frequency values of each target (as deduced from the locations of spectrum peak points), are apart from those of other targets by considerable amount. This situation makes the classification problem at the given frequency range easily solvable. The late-time target responses over the range [46.875-62.5] nsec at reference aspects and the corresponding response-based FFV results are also shown in Figures 4.32, 4.33, 4.34, 4.35 and 4.36 for each target below:

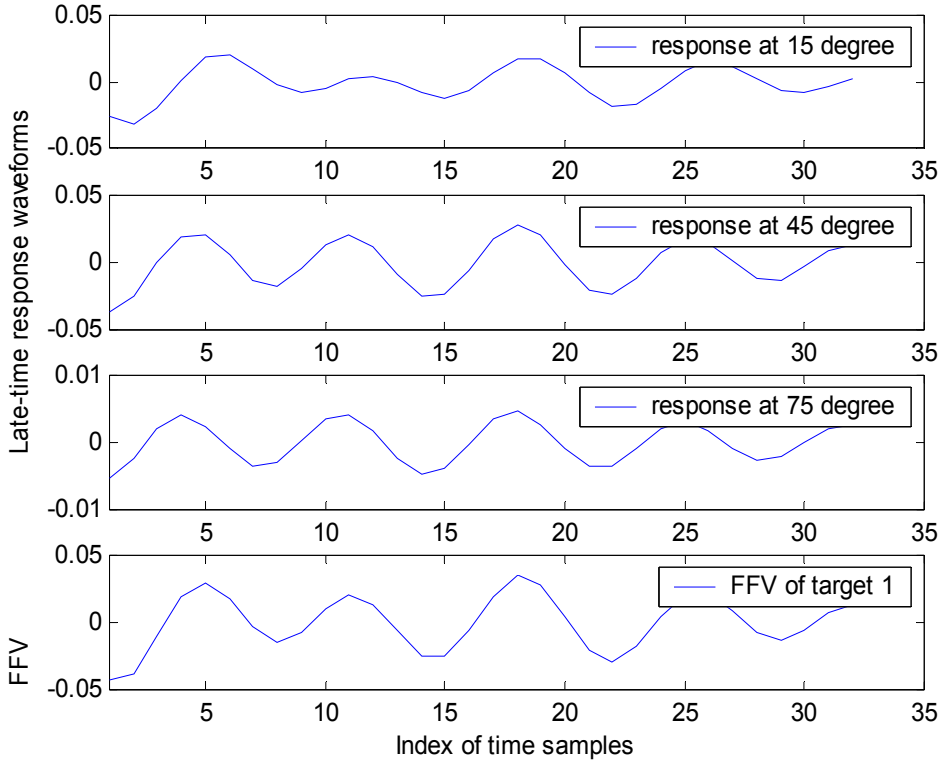

Figure 4.32 Late-time impulse responses for each reference aspect and corresponding FFV of Target 1

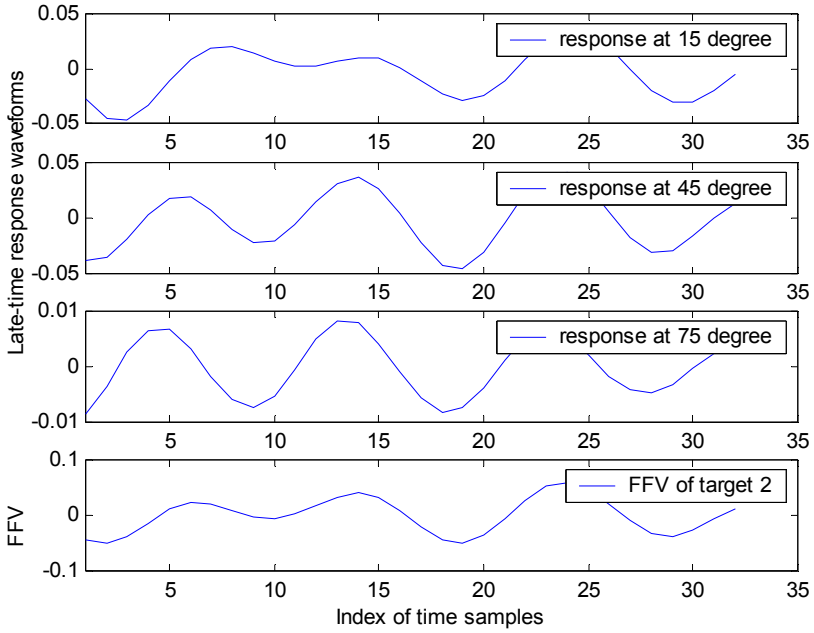

Figure 4.33 Late-time impulse responses for each reference aspect and corresponding FFV of Target 2

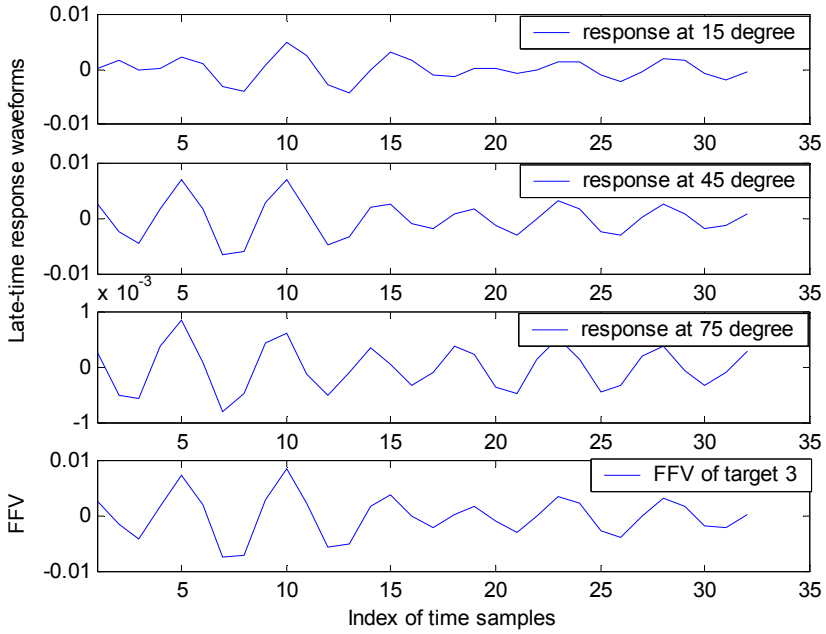

Figure 4.34 Late-time impulse responses for each reference aspect and corresponding FFV of Target 3

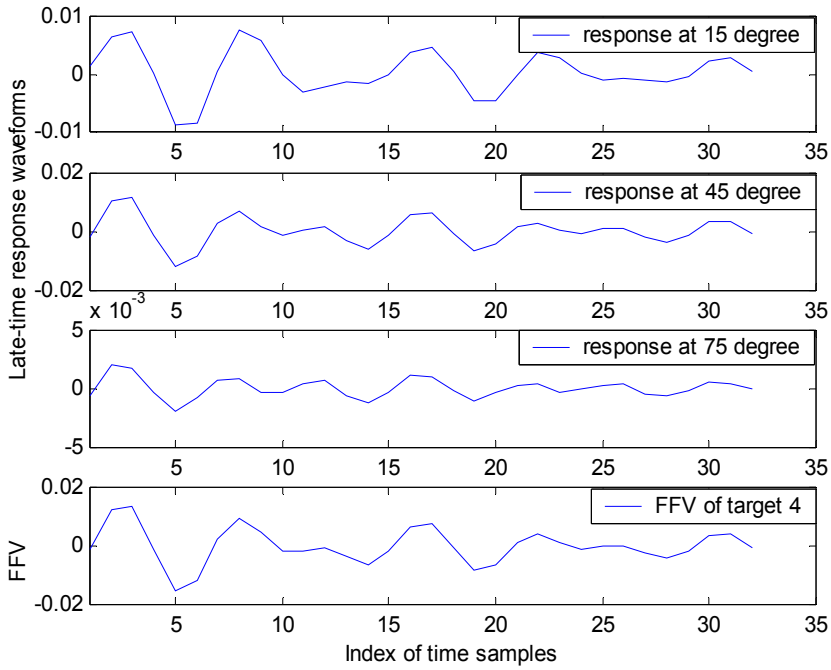

Figure 4.35 Late-time impulse responses for each reference aspect and corresponding FFV of Target 4

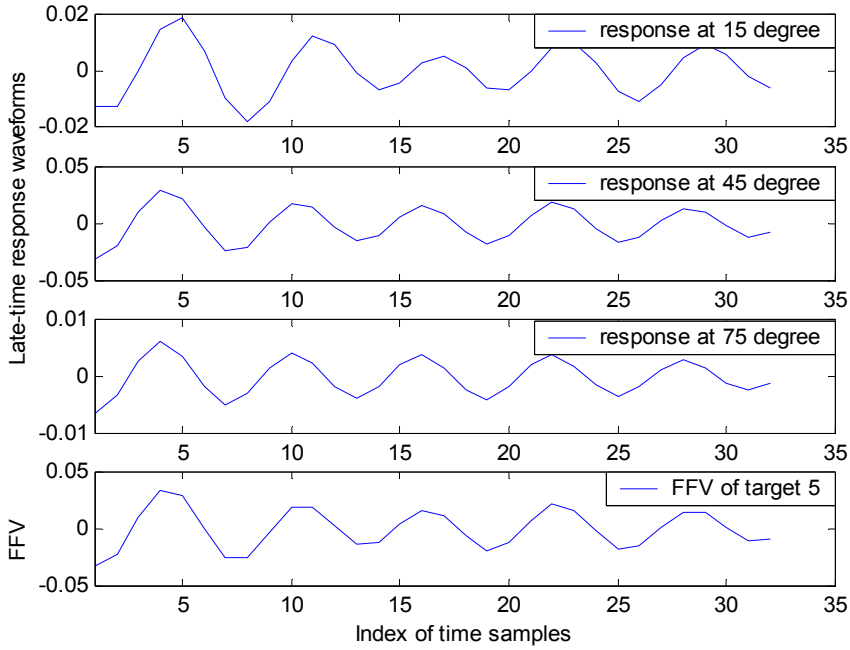

Figure 4.36 Late-time impulse responses for each reference aspect and corresponding FFV of Target 5

In real time, the low detection time is also an important parameter of an electromagnetic target classifier. The FFV based classifier designed for small-scale aircraft targets in this thesis must be tested for this parameter. For this purpose, several back-scattered signals for different targets at test aspects are chosen. Average detection time is calculated as approximately 0.5 sec with (programming in MATLAB environment on a PC with Pentium III, 833 MHz processor). It is a very high detection speed concerning the low speed of the CPU used for computations in this classification problem.

At last, some testing results for the designed FFV based electromagnetic target classifier are given. The back scattered signals of target 1 and target 5 at the aspect angle of $\varphi = 22.5$ degree are used as the test signals. For each test signal, the corresponding LTFVs are extracted properly, and compared with the FFV of each target. Then, the target whose FFV has the highest correlation coefficient with LTFV of the test signal, is selected. In the bar-charts shown in Figures 4.37 and 4.38, the identification results of each test signal are demonstrated, with large safety margins concerning the matched and mismatched correlation coefficient levels.

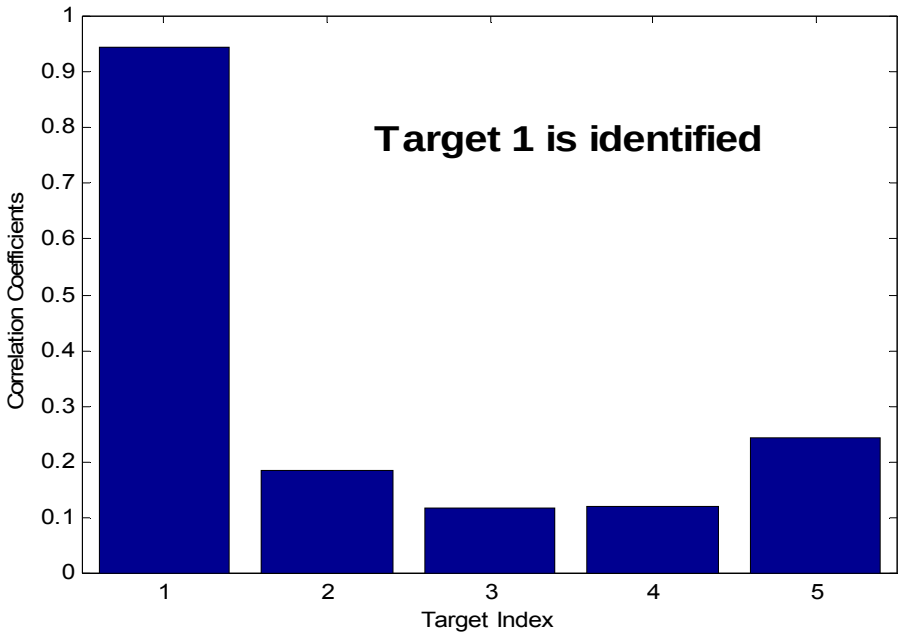

Figure 4.37 The identification of test signal back-scattered at aspect of $\varphi = 22.5$ degree from target 1

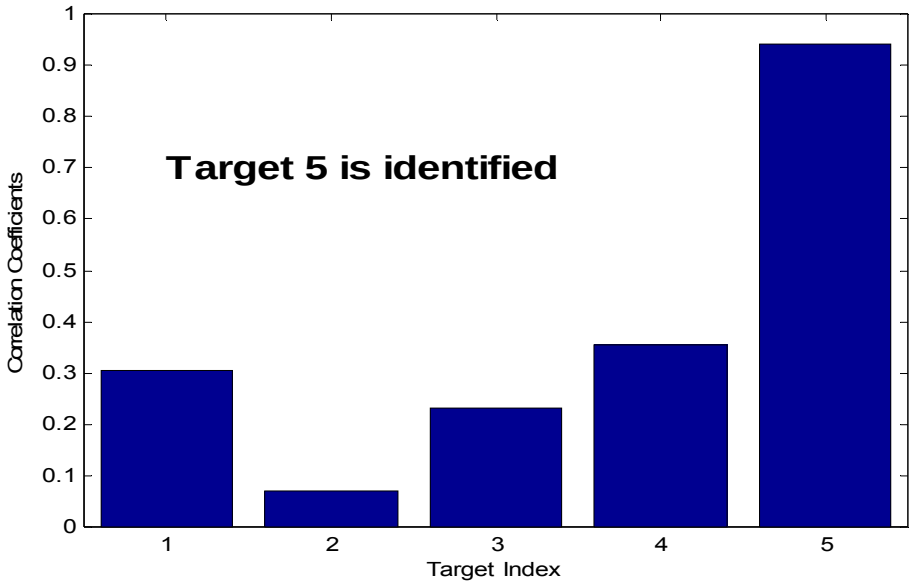

Figure 4.38 The identification of test signal back-scattered at aspect of $\varphi = 22.5$ degree from target 5

CHAPTER 5

CONCLUSIONS

This thesis work has been focused in designing an electromagnetic target classifier for perfectly conducting thin wire structures with moderately complicated geometrical shapes. The fundamental feature extraction technique utilized in this study makes use of the target's natural resonance responses, which convey indirect information about the complex poles of the target's system functions. The target features are extracted from the late-time target responses at only a few different target aspects by the help of two well known signal processing techniques, which are the Wigner Distribution (WD) and the Principal Component Analysis (PCA). The WD is a very useful quadratic time-frequency representation technique used to create the energy distribution maps of scattered signals over the two-dimensional time-frequency domain. Obviously, the late-time portions of these energy distribution maps are very closely related to the real and imaginary parts of the complex resonance frequencies. The PCA technique, on the other hand, is used to fuse multi-aspect features of a given target. Both the WD and the PCA help to extract target features with reduced sensitivity to aspect variations and increased capacity for target characterization. This technique was recently introduced and successfully demonstrated for the classification of loss-free dielectric targets by Turhan-Sayan [1, 2]. Application of the same target classification approach to perfectly conducting targets is studied in this thesis for the first time in literature.

The classifier designed in this work aims to recognize five small-scale aircraft, which are modeled by perfectly conducting, straight, thin wire structures. The realistic aircraft targets are scaled to one percent of their actual dimensions. The criteria looked for in the classifier design problem are high correct decision rates,

computational efficiency in signal processing, small memory requirements for reference database storage and fast decision in real-time.

There was a solid reason for selecting this specific set of aircraft targets: The same target set was used in a recently published paper [7] in the context of electromagnetic target recognition based on the use of full-time scattered responses. The feature extraction technique proposed in that reference was based on the use of Adaptive Gaussian Distribution (a time-frequency representation technique), the PCA technique (used for data reduction purpose in a conventional sense only) and the artificial neural network technique. Although the reported correct classification rates were satisfactorily high, the feature extraction approach used in that paper was very inefficient requiring cumbersome computations, long processing times and an unreasonably large and very closely sampled reference data set. Correct classification rates of about 90 percent were obtained for noise-free or very low noise cases over an aspect range of only 90 degrees at test aspects of 1, 3, 5, 7,…..,89 degrees, by using 46 reference aspects recorded in 0, 2, 4, 6,……90 degrees (measured from the nose-on directions). Our impression was that, when using such an exaggerated number of closely recorded reference aspects, such high target recognition rates could be obtained by even simple interpolation based comparisons, without any need for such complicated signal processing techniques. Therefore, we decided to test our target classifier design technique on the same target set, using exactly the same frequency band and target excitation conditions, to get the comparable or even better correct classification rates while using only 3 reference aspects instead of 46. Indeed, the CCM type correct classification rate of the target classifier designed in this thesis is found to be over 95 percent in noise-free conditions with large safety margins while using only 3 reference aspects (at 15, 45 and 75 degrees) for each candidate target. Using such a small database helps minimizing the memory requirements of the classifier. Furthermore, classification decision in a test case can be completed in less than 0.5 seconds, i.e. in absolutely real-time, using a desktop personal computer with a modest microprocessor of 833MHz speed and running a MATLAB code that was not even optimized for run time efficiency. In summary, we have clearly proven that

the technique used in this thesis is superior to the one proposed in reference [7] in every aspect.

Another interesting conclusion that follows from our classifier design simulations is that the electromagnetic target classifier design technique suggested in references [1, 2] can be further simplified in the case of perfectly conducting thin wire structures such that the WD computation and LTFV extraction steps can be skipped altogether. Instead, the PCA fusion technique can be directly applied to the suitably chosen late-time portions of the target responses to construct the final form of the classifier's feature database. As a future study, validity of this conclusion needs to be searched for perfectly conducting targets of different geometrical shapes.

The electromagnetic classifier design simulations realized in this thesis need to be extended to utilize broader and more realistic frequency bandwidths (to include more of the resonance regime) and to include a extended range of aspect angles (to include the aspects close to the tail parts of the aircraft). Effects of substructures of wire-modeled aircraft targets in classification design may also be studied in future research for better understanding of the overall scattering mechanisms involved.

REFERENCES

[1] G.Turhan-Sayan, "Natural resonance-based feature extraction with reduced aspect sensitivity for electromagnetic target classification", Pattern Recognition, Vol.36, No. 7, pp. 1449-1466, July 2003.

[2] G.Turhan-Sayan, "Real Time Electromagnetic Target Classification Using a Novel Feature Extraction Technique with PCA-Based Fusion" to appear in IEEE Trans. On Antennas and Prop. In Feb.2005.

[3] D.L.Moffatt and R.K.Mains, "Detection and Discrimination of Radar Targets", IEEE Transactions on Antennas and Propagation, vol. AP-23, pp. 358-367, May 1975.

[4] D.P.Nyquist, K.M.Chen, E.Rothwell and B.Drachman, "Radar Target Discrimination using the Extinction-Pulse Technique", IEEE Transaction on Antennas and Propagation, vol. AP-33, pp. 929-937, Sept. 1985.

[5] C.W.Chuang and D.L.Moffatt, "Natural resonances via Prony's method and target discrimination", IEEE Transactions on Aerosp. Electron. Syst., vol. AES-12, 1976.

[6] E.M.Kennaugh, "The K-Pulse Concept", IEEE Transaction on Antennas and Propagation, vol. AP-29, pp. 327-331, March 1981.

[7] K.T.Kim, I.S.Choi, and H.T.Kim, "Efficient radar target classification using adaptive joint time-frequency processing", IEEE Trans. Antennas Propagat., vol. 48, no. 12, pp. 1789-1801, Dec. 2000.

[8] G.Turhan-Sayan, K.Leblebicioglu and T.Ince, "Electromagnetic target classification using time-frequency analysis and neural networks", Microwave and Optical Techn. Lett., vol. 21, no. 1, pp. 63-69, Apr. 1999.

[9] Y.Shi and X.D.Zhang, "A Gabor atom network for signal classification with application in radar target recognition", IEEE Trans. Signal Processing, vol. 49, no. 12, pp. 2994-3004, Dec. 2001.

[10] Azimi-Sadjadi.M.R, De Yao, QiangHuang, Dobeck.G.J, "Underwater target classification using wavelet packets and neural networks", Neural Networks, IEEE Transactions on , Volume: 11 , Issue: 3 , May 2000 Pages:784 – 794.

[11] Jouny.I, Garber.F.D, Ahalt,S.C "Classification of radar targets using synthetic neural networks", Aerospace and Electronic Systems, IEEE Transactions on , Volume: 29 , Issue: 2 , April 1993 Pages:336 – 344.

[12] Xi Miao; Azimi-Sadjadi, M.R.; Bin Tan; Dubey, A.C.; Witherspoon "Detection of mines and minelike targets using principal component and neural-network methods", Neural Networks, IEEE Transactions on, Volume: 9, Issue: 3, May 1998 Pages:454 – 463.

[13] C.E.Baum, "Toward an engineering theory of electromagnetic scattering: the singularity and eigenmode expansion methods", in: P.L.E. Uslenghi (Ed.), Transient Electromagnetic Fields, Academic Press, New York, 1978 (Chapter 15).

[14] Baum,C.E. "Signature-based target identification and pattern recognition", Antennas and Propagation Magazine, IEEE ,Volume: 36 , Issue: 3 , Jun 1994 Pages:44 – 51.

[15] Chi-Chih Chen, "Buried UXO Classification Using the Polarization and Resonance", The Ohio State University ElectroScience Laboratory.

[16] Wei Cher Chen, "Identification of Objects Using Complex Resonances" M.S.Thesis, University of Queensland, School of Information Technology and Electrical Eng, May. 2003.

[17] M.Karaduman, "Use of TFR techniques and the PCA technique in electromagnetic target feature extraction", M.S. Thesis, Middle East Technical University, Electrical and Electronics Eng. Dept, Ankara, Turkey, Dec. 2000.

[18] F.Hlawatsch, G.F.Boudreaux-Bartels, "Linear and quadratic time–frequency signal representations", IEEE Signal Process. Mag. 9 (2) (1992) 21–67.

[19] N.G.Bruijn, "Uncertainty Principals in Fourier Analysis", Academic, New York,1967.

[20] L. Cohen, Time–Frequency Analysis, Prentice-Hall, Englewood Cliffs, NJ, 1995.

[21] J.E.Jackson, A User's Guide to Principal Components, New York: John Wiley & Sons, Inc., 1991.

[22] G.Turhan-Sayan and T. İnce, “Neural Network techniques in Electromagnetic Target Classification: A Comparison Study,” 1999 IEEE AP-S International Symposium and UNSC/URSI National Radio Science Meeting, AP proceedings, Vol.3, pp. 2222-2225, July 1999, Orlando, Florida, USA.

[23] Y.Wang and N.Shuley, “Complex Resonant Frequencies For The Identification Of Simple Objects In Free Space And Lossy Environment”, Progress In Electromagnetics Research, PIER 27, 1-18, 2000.

[24] Stanislav Vitebskiy and Lawrence Carin, “Moment-Method Modeling of Short-Pulse Scattering from and the Resonances of a Wire Buried Inside a Lossy, Dispersive Half- Space”, IEEE Transaction on Antennas and Propagation, vol.43, no.6, November 1995.

[25] FEKO User’s Manual , EM Software & Systems-S.A. (Pty) Ltd, July 2003.

[26] Getting Started Manual , EM Software & Systems-S.A. (Pty) Ltd, July 2003.

APPENDIX A

SOME PROGRAM CODES WRITTEN IN FEKO

FEKO program code to compute the back-scattered frequency responses from target 1 at various aspects, is given below

```
#fmin=4e6
#fmax=256*#fmin
#lammin=#c0/#fmax
#dlen=0.5408
#dlenw=0.4484
#dlent=0.1626
#seg=#lammin/20
#rad=#dlen/2000
#radw=#dlenw/2000
#radt=#dlent/2000
#ld_rate=#dlen/#rad
#check=#seg/#rad
Checking required restrictions:
!!   if #check<4  then
EN
!!endif
Defining edge points:
DP   co                    0        -0.2704   0
DP   cp                    0        0.2704    0
DP   or                    0        0         0
DP   ko                    -0.2242   0        0
```

```
DP   kp                0.2242    0        0
DP   to               -0.0813   -0.2704   0
DP   tp                0.0813   -0.2704   0
```

Constructing wire structures :

```
BL   co   or           #rad      #rad
BL   or   cp           #rad      #rad
BL   ko   or           #radw     #radw
BL   or   kp           #radw     #radw
BL   to   tp           #radt     #radt
EG   1    0    0    0    0
```

Below frequency range and excitation codes are given;

```
FR   256  0            #fmin     #fmin
A0   0        1    1        1        0        60       5        90
DA   0    0    1    0    0    0
FF   -2
FR   256  0            #fmin     #fmin
A0   0        1    1        1        0        60       10       90
DA   0    0    1    0    0    0
FF   -2
FR   256  0            #fmin     #fmin
A0   0        1    1        1        0        60       15       90
DA   0    0    1    0    0    0
FF   -2
FR   256  0            #fmin     #fmin
A0   0        1    1        1        0        60       22.5     90
DA   0    0    1    0    0    0
FF   -2
FR   256  0            #fmin     #fmin
A0   0        1    1        1        0        60       30       90
DA   0    0    1    0    0    0
FF   -2
```

```
FR   256  0              #fmin    #fmin
A0   0       1   1       1       0       60       37.5     90
DA   0   0   1   0   0   0
FF   -2
FR   256  0              #fmin    #fmin
A0   0       1   1       1       0       60       45       90
DA   0   0   1   0   0   0
FF   -2
FR   256  0              #fmin    #fmin
A0   0       1   1       1       0       60       52.5     90
DA   0   0   1   0   0   0
FF   -2
FR   256  0              #fmin    #fmin
A0   0       1   1       1       0       60       60       90
DA   0   0   1   0   0   0
FF   -2
FR   256  0              #fmin    #fmin
A0   0       1   1       1       0       60       67.5     90
DA   0   0   1   0   0   0
FF   -2
FR   256  0              #fmin    #fmin
A0   0       1   1       1       0       60       75       90
DA   0   0   1   0   0   0
FF   -2
FR   256  0              #fmin    #fmin
A0   0       1   1       1       0       60       82.5     90
DA   0   0   1   0   0   0
FF   -2
FR   256  0              #fmin    #fmin
A0   0       1   1       1       0       60       90       90
DA   0   0   1   0   0   0
FF   -2
EN
```

APPENDIX B

SOME PROGRAM CODES WRITTEN IN MATLAB

MATLAB program codes to transform the back-scattered frequency responses to time domain used in this thesis, are given below

```
%ftunw=input('Enter the name of variable that contains freq. data'); % for later use
for arbitrary frequency data
ftunw=eval(s);
load wincodes
ftunw(length(ftunw))=2*real(ftunw(length(ftunw)));
k(1)=0;
for i=2:length(ftunw)+1;
  k(i)=ftunw(i-1);
end
ftunw=k;
clear k i
N=length(ftunw)-1;
for i=1:17;
  if i~=17;   % This if block is used for adding original window W
    l(:,i)=tftb_window(2*N,strcat(wincodes(i,:)));
    w(:,i)=l(N:2*N,i);
    %w(N+1,i)=w(N,i);
  else
    gaussn
    w(:,i)=G';
  end
  ftw(1:N+1,i)=ftunw'.*w(:,i);
  for j=N+2:2*N;
    ftw(j,i)=ftunw(2-j+2*N)*w(2-j+2*N,i);
  end
    testsignal(:,i)=real(ifft(conj(ftw(:,i))));
    testsignaln(:,i)=testsignal(:,i)/(sqrt(sum(testsignal(:,i).^2)));%making energy be
unity
    %Output display type return to next one
    %figure(i);
    %plot(testsignal(:,i));
    %title(strcat('Using window type:  ',wincodes(i,:)));
```

```
    %pause
    %delete(i)
end
%testsignal=testsignal'; % Just to prevent chaos :)
%testsignaln=testsignaln';
sig=testsignal(:,17); % Output ready to use in hdis family
sign=testsignaln(:,17);
%plot(sig)

*****************************************************

% GAUSSIAN WINDOW CODE

clear f G;
pi=3.141592654;

%ftres=input('Enter treshold freq. in MHZ')
ftres=1000;
%magtres=input('Enter treshold window magnitude %')
magtres=0.01;

% COMPUTE VARIANCE

b=-log(magtres);

sigma=sqrt(2*b)/(2*pi*ftres);

%delf=input('Enter freq. step in MHz.')
delf=4;
%fst=input('Enter start freq. in Ghz.');
fst=0;
%NFFT=input('Enter N for N-point fft');
NFFT=512;

NF=1+NFFT/2;

for k=1:NF
  f(k)=fst+(k-1)*delf;
  G(k)=exp(-0.5*(sigma*2*pi*f(k))^2);
end;

ktresh=((ftres-fst)/delf)+1;
treschk=G(ktresh);

%v=axis([0,f(NF),0,1]);
%ephitn_noisytplot(f,G)
load wincodes
ll=tftb_window(NFFT,strcat(wincodes(11,:)));
```

ww=ll(NFFT/2:NFFT);

MATLAB program codes to obtain LTFVsused in this thesis, are given below

```
clear all
load Qval
load Ntimecut
const='ucak';
for m=1:5;
  j=[5 10 15 22 30 37 45 52 60 67 75 82 90];
  n=num2str(m);
    for r=j;
    r=num2str(r);
    load(strcat(const,n,'_60_',r,'_1024','time'));
    s=strcat(const,n,'_60_',r,'_1024','time');
    x=eval(s);
    N=length(x);
    [a,b,c]=tfrwv(x,1:N,N);
    a=(a+abs(a))/2;
    d=a(1:(N/2),1:N/Ntimecut);
    q=Qval;
    for i=1:q;
      se(:,i)=sum(d(:,(((i-1)*(N/Ntimecut)/q)+1):(i*(N/Ntimecut)/q)),2);
    end
    secol(1:q*N/2)=(q/(N/Ntimecut))*se;
    late1112=secol(((3*length(secol)/Qval)+1):(4*length(secol)/Qval));
    assignin('base',strcat(s,'fv'),late1112);
    save(strcat(s,'fv'),strcat(s,'fv'))
  end
end
```

****

MATLAB program codes to obtain FFVs are given below

```
%These lines are executed only once for obtaining pca data
clear all
const='ucak'
for i=1:5;
  m=num2str(i);l=0;
  for j=[15 45 75];
    k=num2str(j);l=l+1;
    load(strcat(const,m,'_60_',k,'_1024','timefv'));
    pcaint(l,:)=eval(strcat(const,m,'_60_',k,'_1024','timefv'));
  end
  assignin('base',strcat('pcaint',m),pcaint);
  save(strcat('pcaint',m,'.dat'),'pcaint','-ascii')
  [a b c d]=princomp(eval(strcat('pcaint',m))');
  assignin('base',strcat('pca',m),b(:,1)');
  save(strcat('pca',m,'.dat'),strcat('pca',m),'-ascii')
  pca(i,:)=eval(strcat('pca',num2str(i)));
  save(strcat('pca','.dat'),'pca','-ascii')
  %keyboard
end
%clear i j k m l a b c d pcaint
```

MATLAB program codes to obtain CCM type correct decision rates are given below

```
clear
const='ucak';
load pca.dat;
%m= input('select test target plane number','s');
%k=input('select angle of phi','s');
for m=1:5;
  j=[5 10 15 22 30 37 45 52 60 67 75 82];
  n=num2str(m);
  for r=j;
    r=num2str(r);l=0;
    load(strcat(const,n,'_60_',r,'_1024timefv'));
    %testing target type
    for i=1:5;
      test_coef(i)=corr2(eval(strcat(const,n,'_60_',r,'_1024timefv')),pca(i,:));
    end
    [a,b]=max(test_coef);
    if b~=m
      fprintf(1,strcat('Wrong identification:  ',num2str(b),'   instead of ',num2str(m),'
at phi= ',r,'\r'));
      l=1;
    end
    %for block below written for CCM %25 criteria
    if l ~= 1
      for c=1:5;
        if b~=c
          if test_coef(c) >= 0.75*test_coef(b)
            fprintf(1,strcat('Wrong identification CCM5:  ',num2str(c),'   instead of
',num2str(b),' at phi= ',r,'\r'));
          end
        end
      end
    end
    %fprintf(1,strcat('Identified Target Type :',num2str(b),'\r'));%for output screen
display
  end
end
```